NATIONAL ADVISORY COMMITTEE FOR AERONAUTICS

TECHNICAL NOTE 3338

A DYE-TRACER TECHNIQUE FOR EXPERIMENTALLY OBTAINING IMPINGEMENT CHARACTERISTICS OF ARBITRARY BODIES AND A METHOD FOR DETERMINING DROPLET SIZE DISTRIBUTION

By Uwe H. von Glahn, Thomas F. Gelder, and William H. Smyers, Jr.

Lewis Flight Propulsion Laboratory
Cleveland, Ohio

Washington
March 1955

NATIONAL ADVISORY COMMITTEE FOR AERONAUTICS

TECHNICAL NOTE 3338

A DYE-TRACER TECHNIQUE FOR EXPERIMENTALLY OBTAINING IMPINGEMENT CHARACTERISTICS OF ARBITRARY BODIES AND A METHOD FOR DETERMINING DROPLET SIZE DISTRIBUTION

By Uwe H. von Glahn, Thomas F. Gelder
and William H. Smyers, Jr.

SUMMARY

A dye-tracer technique has been developed whereby the quantity of dyed water collected on a blotter-wrapped body exposed to an air stream containing a dyed-water spray cloud can be colorimetrically determined in order to obtain local collection efficiencies, total collection efficiency, and rearward extent of impingement on the body. In addition, a method has been developed whereby the impingement characteristics obtained experimentally for a body can be related to theoretical impingement data for the same body in order to determine the droplet size distribution of the impinging cloud. Several cylinders, a ribbon, and an aspirating device to measure cloud liquid-water content were used in the studies presented herein for the purpose of evaluating the dye-tracer technique. Although the experimental techniques used in the dye-tracer technique require careful control, the methods presented herein should be applicable for any wind tunnel provided the humidity of the air stream can be maintained near saturation.

INTRODUCTION

In the design and evaluation of thermal icing protection systems for aircraft, one of the more important factors in the determination of heating requirements and the chordwise extent of heated area is the cloud-droplet impingement characteristics of the various components requiring protection. Previous investigations (refs. 1 to 11) have generally been confined to analytical solutions of the droplet impingement characteristics. These solutions involve the use of differential analyzers or mechanical analogs for computation of the droplet trajectories once the flow field about the component has been calculated. Bergrun determined a limited number of trajectories for an airfoil in

reference 4 using step-by-step calculations. In addition, in reference 12 Bergrun derived an empirical method permitting estimation of the droplet impingement characteristics on arbitrary airfoil sections. This method, however, appears to be more applicable to Joukowski-type airfoils than to low-drag or high-speed airfoils because the basic data used in developing the method were obtained for four Joukowski airfoil sections, but for only one low-drag section.

Because of the labor and time required to calculate the complex flow fields about some bodies and the droplet trajectories through these flow fields, it is often impractical to obtain droplet impingement characteristics theoretically. It is therefore desirable to obtain an experimental method for the determination of droplet impingement characteristics and thereby avoid the calculation of complex flow fields.

A series of investigations were initiated at the NACA Lewis laboratory and under NACA contract at the Daniel Guggenheim Airship Institute (Univ. Akron) to determine a suitable means for experimentally studying droplet impingement characteristics on a body at above-freezing air temperatures. Initial studies at the University of Akron were concerned with developing a technique to obtain a record or trace of droplet impingement on an arbitrary body. Subsequent studies at the Lewis laboratory were concerned with improvements in the technique and the correlation of experimental impingement results with theoretical studies. Because available instruments were inadequate to determine accurately droplet size distributions, a method was developed by which the droplet size and distribution in the cloud were ascertained from impingement records on several bodies for which the theoretical trajectories are available.

This report presents a description of tracer techniques developed by the NACA to obtain the experimental impingement characteristics of arbitrary bodies. In addition, a method is presented for applying theoretical impingement data (refs. 1 and 2) to the experimental impingement data from cylinders to determine the droplet size distribution of the impinging cloud. A review of basic impingement relations precedes the main body of the report to clarify and provide a basis for the development of the methods herein described.

BASIC IMPINGEMENT RELATIONS

A body moving through a cloud of water droplets will not, in general, intercept all the droplets originally contained in the volume of air swept out by the projected frontal area of the body. If the body is considered to be fixed in a reference system, then, at a large distance ahead of the body, the droplets and the air both approach in straight line paths with a free-stream velocity V_0. (All symbols used

herein are defined in appendix A.) As the droplets and the air reach the vicinity of the body, the air streamlines deviate from their original straight line paths and flow around the body. The air flow field is dependent primarily on the shape of the body and the orientation of the body with respect to the direction of the free-stream velocity. A droplet, because of its momentum, tends to maintain its original straight-line path toward the body; however, the drag force imposed by the relative velocity of the air with respect to the droplet as the air streamlines deviate tends to cause the droplets to follow the air streamline. The combined effect of the momentum and the drag determines the trajectory of the droplet. For the case of small droplet size, high air viscosity, low free-stream velocity, and high air density, the effect of the droplet drag will exceed that of the droplet momentum; consequently, the droplets will tend to follow the curved streamlines around the body. In this case, many of the droplets which were originally directly ahead of the frontal area of the body will miss the body entirely. For the condition of large droplets, low air viscosity, high free-stream velocity, and low air density, the effect of the momentum is greater than that of the drag, and the droplets will tend to maintain their original straight-line trajectories. For this case, only a few of the droplets which were originally directly ahead of the frontal area of the body will diverge enough from their straight-line paths to miss the body.

The basic differential equations of motion for a droplet in an air stream approaching a body are presented in dimensionless form in references 1 to 3. For a body configuration where shape and orientation with respect to free-stream velocity direction are given but size is variable, the theoretical trajectory of a droplet is determined by any two of the four impingement parameters K, φ, Re_0, and ψ. These dimensionless parameters are interrelated ($K\varphi = Re_0^2$, $\psi^2 = \varphi/K$) and include such factors as droplet size, body size, air viscosity, droplet density, air density, and free-stream velocity (appendix A).

Body of arbitrary shape in cloud of uniform drop size. - The basic definitions of the dependent impingement parameters - limit of impingement, total collection efficiency, and local collection efficiency - can be expressed in general equations for bodies of arbitrary shape and orientation. A general case for impingement considerations is that of an arbitrary body placed in an incompressible air stream which contains droplets of uniform size. For simple bodies, the flow field may be expressed mathematically, and the equations of droplet motion may be solved by the use of a mechanical analog or a differential analyzer. The direct result of these computations is a trace of the droplet trajectory for each initial ordinate measured from a reference line at an infinite distance ahead of the body. For illustrative purposes, the droplet trajectories for a simple two-dimensional body are shown in figure 1. The

dashed traces represent typical trajectories for a fixed set of impingement conditions (described by K and φ). The solid lines are typical traces for another set of conditions (other values of K and φ) for which the momentum effect is greater and the droplet follows a straighter trajectory. For a given set of K and φ conditions, the droplets which start out at progressively larger initial ordinates (y_0's) will strike the body progressively farther back along the surface until a maximum value $y_{0,m}$ is obtained. The trajectory starting at $y_{0,m}$ will be tangent to the surface of the body at point p, which is a distance s_m (measured along the surface) from a reference point on the body. All droplets which have initial ordinates greater than $y_{0,m}$ at an infinite distance ahead of the body ($x = -\infty$) will miss the body completely. Therefore, s_m denotes the distance along the body surface to the limit of impingement or the point on the surface beyond which no droplets will impinge. For arbitrary three-dimensional bodies the rearward limit of impingement will vary everywhere around the surface periphery.

For an arbitrary three-dimensional body in a cloud of uniform droplet size, the total collection efficiency E_m is defined as:

$$E_m = \frac{\text{(amount of water caught in a unit of time by a body)}}{\text{(amount of water which could be caught in that unit of time if the trajectories were all straight lines parallel to the free-stream velocity direction)}} \tag{1}$$

or

$$E_m = \frac{A_{0,m}}{A_f} \tag{2}$$

where A_f is the projected frontal area of the body and $A_{0,m}$ is the area through which all the droplets hitting the body must pass at some point a large distance ahead of the body, both areas being normal to the free-stream velocity direction. If the numerator of equation (1) is denoted as the total water collection rate W_m (lb/hr), the equation may be written as:

$$W_m = 0.329\, V_0\, w_t\, A_f\, E_m \tag{3}$$

The local collection efficiency β for specified impingement conditions (K, φ) is defined for any point on the body surface as:

$$\beta = \frac{\text{(amount of water caught on infinitesimal area of surface in a given unit of time)}}{\text{(amount of water which could be caught in that time on that area if the trajectories were straight lines parallel to the free-stream velocity direction and if the area were oriented to be perpendicular to the trajectories)}} \tag{4}$$

or

$$\beta = \lim_{\Delta A_s \to 0} \frac{\Delta A_0}{\Delta A_s} = \frac{dA_0}{dA_s} \tag{5}$$

where ΔA_s is an increment of area on the surface of the body and ΔA_0 is the increment of A_0 (which is the area perpendicular to the air stream) through which all the droplets impinging on ΔA_s must pass. The value of β at any point on the body determines the local impingement rate W_β, defined as the amount of water collected on a small area at that point per unit time. In terms of the local collection efficiency, W_β is defined as:

$$W_\beta = 0.329 \, V_0 \, w_t \, \beta \tag{6}$$

The β values over the surface are also useful in some instances for the determination of the total collection efficiency E_m. An integration of the local collection efficiencies over the surface area subject to impingement and division by A_f yields the following relations:

$$\frac{1}{A_f} \int \beta \, dA_s = \frac{1}{A_f} \int \frac{dA_0}{dA_s} \, dA_s = \frac{A_{0,m}}{A_f} = E_m \tag{7}$$

If equation (7) is multiplied by $0.329 \, V_0 \, w_t \, A_f$, it is apparent from equations (3) and (6) that

$$\int W_\beta \, dA_s = W_m \tag{8}$$

Effect of nonuniform droplet size distribution on impingement parameters. - In many cases droplets of various sizes are intermingled in a cloud whether it is naturally or artificially produced. Various graphical representations may be employed to describe the distribution of droplet sizes in a cloud; these representations employ either (1) a block-type distribution or (2) a smoothly faired distribution curve. These

droplet size distributions are often shown as the variation of cumulative liquid-water content w as a function of droplet radius a. The dimensionless form of their plot is $n = w/w_t$ as a function of a/a_{med}. By definition, the volume-median droplet size a_{med} is that droplet size for which half the total liquid-water w_t is contained in droplets larger than a_{med} and half the total water is contained in droplets smaller than a_{med}.

A series of dimensionless hypothetical block distributions is presented in reference 2; an example of such a distribution (Langmuir D-type) is shown in figure 2 together with a smooth curve approximation. Both block and faired curve droplet size distributions may be employed in the analysis of the impingement of cloud droplets on various bodies; the choice is in most cases a matter of convenience.

The dimensionless dependent impingement paramaters s_m/L, E_m, and β for a body in a cloud of nonuniform droplet size must be treated in a manner somewhat different from those for a body in a cloud of uniform droplet size. The limit of impingement, which can be denoted by s_m/L for a single droplet size, must now be defined as the limit of impingement caused by the maximum droplet size present in the cloud, and is therefore denoted as $(s_m/L)_{max}$. The parameters denoted by β, W_β, E_m, and W_m for the case of a single droplet size are weighted to account for the effect of all droplet sizes present in the distribution. The weighted paramaters used with a droplet size distribution are denoted herein as $\overline{\beta}$, $\overline{W}_\beta$, $\overline{E}_m$, and $\overline{W}_m$.

The process of weighting these parameters when the droplet distribution is specified and the theoretical dependent impingement parameters s_m/L, β, and E_m are known as a function of the independent impingement parameters K and φ is an averaging process. This process defines $\overline{E}_m$ and $\overline{\beta}$ so that the equations

$$\overline{W}_m = 0.329\, A_f\, \overline{E}_m\, V_0\, w_t \tag{9}$$

and

$$\overline{W}_\beta = 0.329\, V_0\, w_t\, \overline{\beta} \tag{10}$$

are satisfied. Equations (9) and (10) for a nonuniform droplet size distribution correspond to equations (3) and (6), respectively, for a distribution of uniform droplet size.

If a cloud of block-type distribution such as the solid lines in figure 2 (with a_{med} and w_t specified) impinges upon a given body for which theoretical trajectory calculations are available, the weighted total collection efficiency $\overline{E}_m$ may be defined as an average E_m:

$$\overline{E}_m = \frac{1}{w_t}\left(E_{m,1}\,\Delta w_1 + E_{m,2}\,\Delta w_2 + \cdots E_{m,7}\,\Delta w_7\right)$$

$$= E_{m,1}\,\Delta n_1 + E_{m,2}\,\Delta n_2 + \cdots E_{m,7}\,\Delta n_7 \qquad (11)$$

Every droplet size group in figure 2 has a corresponding finite value of partial water content Δw (or Δn) and droplet size a. For given operating conditions, every droplet size specifies a K value which, along with φ, determines E_m for that droplet group. These E_m values may be then used in equation (11) to determine $\overline{E}_m$. Equation (11) may be graphically represented by a summation of the areas in figure 3(a).

If a faired-type distribution such as the dashed line in figure 2 is specified, equation (11) takes the form:

$$\overline{E}_m = \frac{1}{w_t}\int_{w=0}^{w=w_t} E_m\,dw = \int_{n=0}^{n=1} E_m\,dn \qquad (12)$$

For this type distribution E_m may be plotted as a function of w (or n) as in figure 3(b) and integrated graphically to obtain $\overline{E}_m$. Then $\overline{W}_m$ may be determined from equation (9).

The weighting of local impingement rate parameters such as β or W_β is accomplished in the same manner as the weighting of E_m except that the averaging process must take place at every point on the surface of the body where $\overline{\beta}$ is desired since β varies along the surface of the body. The quantity $\overline{\beta}$ is the average β at the particular location under consideration for all the droplets in the cloud.

If a cloud containing a block-type distribution, such as that represented by the solid lines in figure 2, impinges upon a body the weighted local collection efficiency $\overline{\beta}$ may be defined as

$$\overline{\beta} = \frac{1}{w_t}\left(\beta_1\,\Delta w_1 + \beta_2\,\Delta w_2 + \cdots + \beta_7\,\Delta w_7\right)$$

$$= \beta_1\,\Delta n_1 + \beta_2\,\Delta n_2 + \cdots + \beta_7\,\Delta n_7 \qquad (13)$$

Equation (13) results in the $\bar{\beta}$ value at only one surface location since β is a function of droplet size and surface location. If $\bar{\beta}$ is to be determined over the entire area of droplet impingement on the body, equation (13) must be applied at enough surface points on the body to evaluate $\bar{\beta}$ as a function of location s. Equation (13) is graphically represented in figure 4 for the surface location s_0 on a two-dimensional body. The value of $\bar{\beta}$ is obtained by the summation of $\beta\Delta n$, which is equal to the cross-hatched area in figure 4. For other surface locations (s_1, s_2, s_3, etc. in fig. 5) successively farther back from the reference point, equation (13) is likewise applied and $\bar{\beta}$ at s_n is the area under that s_n curve. There is a limit of impingement s_m for each droplet size group (each Δn). This limit is determined by the K and φ for each group. For surface distances on the body greater than s_m for any group, the β for that group equals zero. As the surface distance from the reference point increases ($s > s_0$), only the groups of increasingly larger droplet sizes will contribute to $\bar{\beta}$, as shown in figure 5. By summing under each s_n curve of figure 5, the $\bar{\beta}$ value for that location is determined as previously illustrated in figure 4. This procedure of summing for $\bar{\beta}$ for each location s_n results in a plot (see fig. 6) of $\bar{\beta}$ as a function of surface distance for one set of operating conditions. If a smooth droplet size distribution curve is specified, equation (13) takes the form

$$\bar{\beta} = \frac{1}{w_t} \int_{w=0}^{w=w_t} \beta \, dw = \int_{n=0}^{n=1} \beta \, dn \tag{14}$$

Equation (14) may be applied at several surface locations (s_n) as graphically represented in figure 7. The area under any s_n curve in figure 7 represents $\bar{\beta}$ for that surface location, and therefore $\bar{\beta}$ may be shown as a function of s as in figure 8. Figures 7 and 8 for the smooth-type droplet size distribution curve are comparable to figures 5 and 6, respectively, for the block-type distribution curve.

Weighted local impingement rate $\bar{W}_\beta$ and weighted local collection efficiency $\bar{\beta}$ may be integrated over the surface of the body to produce the total impingement rate $\bar{W}_m$ and total collection efficiency $\bar{E}_m$, respectively:

$$\bar{W}_m = \int \bar{W}_\beta \, dA_s \tag{15}$$

$$\bar{E}_m = \frac{1}{A_f} \int \bar{\beta} \, dA_s \tag{16}$$

Equations (15) and (16) for the cloud of nonuniform droplet size correspond to equations (8) and (7), respectively, for the case of uniform droplet size.

GENERAL DESCRIPTION OF EXPERIMENTAL APPROACH

The objectives of an experimental droplet impingement study are the evaluations of total collection efficiency of a body, the local collection efficiency around the surface, and rearward extent of droplet impingement on the body. The method described herein to determine these quantities experimentally consists of a measurement of the local impingement rate $\bar{W}_\beta$ on a body. The measurement is obtained from a dye deposit left on the body. The amount of dye deposit is directly proportional to the water impingement rate. In this technique, water treated with small quantities of water-soluble dye is injected in the form of droplets into the air stream ahead of the body by means of spray nozzles. The surface of the body is covered with an absorbent material upon which the dyed water impinges and is absorbed. At the point of impact and droplet absorption, a permanent dye deposit (hereinafter designated as dye trace) is obtained. The amount of dye trace obtained in a measured time interval can be determined by colorimetric analysis and converted into the quantity of water which produced it if the composition of the treated water is known.

The impingement limit s_{max} is obtained directly from the rearmost dye trace (where $\bar{M}_\beta \rightarrow 0$). The dye analysis consists of removing the dye impregnated absorbent material from the body and punching out small segments of the material for the determination of local impingement characteristics. The dye is dissolved out of each segment in a known quantity of water. The weight of dye in this solution is determined by the amount of light of a suitable wave length that will be transmitted through the solution by use of a calibrated colorimeter. From a knowledge of the original concentration of the dye in the water droplets, the weight of dye collected per unit area can be converted into the weight of water which impinges at any surface location per unit time. This conversion assumes that no evaporation of the dyed droplets occurred in the air stream. The use of the experimental local impingement rates $\bar{W}_\beta$ to evaluate $\bar{E}_m$ was discussed in the previous section.

The determination of the droplet size distribution from the experimental local impingement rates on a body requires a thorough knowledge of the theoretical droplet trajectories around the body (discussed in a subsequent section). A survey of the available literature indicated that the most reliable and abundant theoretical impingement data existed

for two-dimensional bodies such as airfoils, cylinders, and ribbons. Of these data the cylinder analysis (refs. 1 and 2) appeared to be the most applicable for an experimental study that required an accurate determination of local impingement rates from the dye traces. The impingement data reported herein were therefore obtained by analyzing the impingement records from several different sized cylinders.

APPARATUS

Models and related equipment. - The experimental studies of droplet impingement characteristics on cylinders were conducted in the 6- by 9-foot test section of the NACA icing tunnel. Three wooden cylinders all of 1-foot span and 2, 4, and 6 inches in diameter were installed on a hydraulically actuated elevator shaft. End plates were used on all cylinders to maintain two-dimensional flow characteristics over the model. The cylinders were moved in and out of the tunnel by means of the elevator. A photograph of the 4-inch cylinder mounted in the center of the tunnel test section is shown in figure 9.

Pressure distributions for the 2- and 6-inch cylinders were obtained by means of pressure belts cemented to the cylinder surface.

A square grid made up of 1/8- by 1/2- by 24-inch bar stock held ribbons which were used for measuring cloud uniformity and was mounted in the tunnel test section as shown in figure 10. An aspirating device was used to determine the cloud liquid-water content and is described in appendix B.

Absorbent material. - The absorbent material selected for the studies had to satisfy three basic requirements: (1) The material must have the capacity to absorb and hold at the point of impact an amount of dyed water sufficient to produce adequate color contrast for good colorimetric determinations, (2) the thickness of the material must be such that it can be readily formed without breaking or otherwise distorting the model contours and be of negligible thickness as compared with the dimensions of the model, and (3) the material must have no perceptible chemical reaction with the dye solution. For the studies herein, commercial varieties of white blotter paper of two thicknesses, 0.017 inch and 0.023 inch, were used; however, for the models and spray conditions investigated no difference in results was obtained with the two thicknesses.

Ribbons of blotter paper 1/8 by $1\frac{1}{2}$ inch were fastened to the leading edge of the grid bar stock for use in measuring the cloud uniformity at various locations throughout the cross-sectional area determined by the grid dimensions. An accurately machined paper punch was used to

obtain these ribbons (1/8 by $1\frac{1}{2}$ in.) from sheets of blotter paper. Blotters about 3 inches wide were fastened to the three cylinder models by means of masking tape mounted parallel to the cylinder axis and downstream of the maximum thickness point.

Dye and water for spray fluid. - A dye that would provide impingement records suitable for analysis was selected to satisfy the following criteria: (1) The dye must be readily and completely soluble out of the absorbent material; (2) the dye must be nonvolatile to prevent dye losses from the trace to the surrounding air by evaporation after exposure to the spray; (3) the dye must be reasonably color fast and chemically stable so that the trace will not fade or otherwise change in chemical nature during processing; (4) the solution of dye in the spray fluid must be a true solution and must provide sufficient color contrast on the absorbent material to allow accurate colorimetric analysis and determination of the limit of impingement from the rearmost dye trace; (5) the dye should be substantially pure to eliminate the possibility of impurities settling out of solution, and should be chemically inert to eliminate any reaction with the spray system piping.

Of the dyes that would satisfy these criteria, a red dye of the azo group (Carmoisine BA Extra Conc. 118 percent factory strength, General Dyestuff Corp.) was chosen for the experimental studies reported herein. Water-dye solutions between 0.5 and 1.0 percent dye by weight were studied and proved satisfactory with respect to solubility and color contrast. The 0.5 percent (nominal) dye in water solution was used throughout this investigation. A standard colorimeter was used to determine the light transmittal characteristics of the water-dye solutions. For colorimetric analysis with a nearly monochromatic light source, the best color definition for the dye-water solution was obtained at a wavelength of 520 millimicrons.

Distilled water was used throughout this investigation. In order to obtain a true solution of dye in the spray water, the dye-water solution was agitated mechanically and heated for several hours near the boiling point. The addition of carbon dioxide to the distilled water to make the water slightly acidic seemed to improve the stability of dye-water solutions made with the water.

Spray system. - For the purposes of the present study a special spray system was used containing four air-water atomizing nozzle assemblies of the type shown in figure 11. The nozzle assembly consists of (1) a two-way, fast action, normally-closed solenoid valve, (2) the spray nozzle (Inconel), and (3) the nozzle housing which contains the atomizing air inlet. These nozzles are of the same design as those used

in the main icing spray system of the icing tunnel and are located in the same low-air-velocity section of the tunnel. Each of the nozzle assemblies was adjustable as to its orientation, facilitating the development in the tunnel test section of a spray cloud that was uniform in liquid-water content and of sufficient size to cover completely the largest model studied. The dye solution was pressurized (100 and 120 lb/sq in.) in a 15 gallon Inconel supply tank. From the tank, the solution passes through stainless steel tubing and fittings to a stainless steel manifold and thence through rubber hoses to each individual nozzle assembly. (Inconel, stainless steel, and rubber were unaffected by the dye solution; whereas other materials, including brass, copper, and aluminum, reacted chemically with the dye solution.) The air used for the spray nozzles is pressurized (60-80 lb/sq in.) and is nearly saturated with water vapor. This air, after passing through a porous filter for cleaning, is ducted to a steel manifold and then through rubber hoses to each nozzle assembly to be discharged through the nozzle orifice (fig. 11) at sonic velocity.

Calibration of the spray system and valve-triggering mechanism indicated no measurable time lag in the opening and closing of the valve. Increasing the air-water pressure ratio from 0.5 (60 lb/sq in. air, 120 lb/sq in. water) to 0.6 (60 lb/sq in. air, 100 lb/sq in. water) and then to 0.8 (80 lb/sq in. air, 100 lb/sq in. water) resulted in a decreased water flow rate. A low water flow rate for the air and water pressures used is accompanied by a small droplet size, whereas a large water flow rate is accompanied by a large droplet size.

Air and spray-fluid pressure were remotely and independently controlled from the main icing tunnel control room by means of suitable pressure regulators and transmitters. These pressures were recorded by means of a manometer board. All pressures were preset and could be repeated and maintained within ±1/2 pound per square inch. The solenoid valves which controlled the spray duration were linked to an electronic timer by means of which the duration of the spray was repeatable to ±0.02 second.

PROCEDURE

Conditioning of tunnel air stream. - The studies reported herein were conducted at a nominal free-stream velocity of 175 miles per hour, a total air temperature ranging from 45° to 60° F, and a pressure altitude of approximately 28.2 inches of mercury. The tunnel air stream was conditioned to be as nearly saturated as possible before the body was exposed to the dyed-water spray. This procedure minimized the evaporation of water from the droplets during their time of travel (less than 1 sec) from the spray nozzles to the body. (The absence of evaporation

was verified by weighing a ribbon on an analytical balance immediately after exposure and comparing the actual amount of water caught with the amount calculated by the dye technique.) A nearly saturated air condition was achieved through the control of tunnel air temperature and the addition of steam to the air stream. Indication of a nearly saturated air stream was obtained visually from the formation of a light condensation cloud in the tunnel test section prior to exposing the models to the dyed-water spray. Previous studies had shown that the presence of a light condensation cloud in the test section was accompanied by a relative humidity above 90 percent at the spray system; this humidity evaluation was made with a psychrometer.

Exposing of models to spray cloud. - The procedure for each run was to preload the air and dyed-water pressure in the spray system, preset the exposure time, and then, with the tunnel air properly conditioned as to speed, temperature, and relative humidity, lower the cylinder with blotter attached into the center of the test section. In the case of the ribbons, the grid was mounted in the center of the tunnel during the air stream conditioning process. The solenoid valves in the spray nozzle assembly (see fig. 11) were then energized to permit the flow of dyed water into the air stream for the preset and automatically recorded time interval. The models were then removed from the tunnel.

The exposure time for the ribbons and cylinders was varied with both the model size and water content in the cloud. A long exposure in the spray cloud (soggy blotter) causes lateral dispersion of dyed water in the blotters resulting in erroneous impingement rates. Excessively long exposures also permit the dyed water to soak through the blotter paper onto the body, resulting in a loss or redistribution of dyed water. In the studies described herein, a satisfactory exposure time for the ribbons was less than 3 seconds and for the cylinders ranged from 4 to 10 seconds at air-water pressure ratios of 0.5 to 0.8, respectively.

Spray cloud calibration. - Analysis of the dye collected by the ribbons on the grid determined the uniformity and reproducibility of the spray cloud. The amount of dye collected on the grid ribbons was relatively constant (±5 percent) for the portion of the cloud that covered a cross-sectional area in the test section greater than the frontal area of the largest (6-in. diam.) cylinder. This uniform portion of the spray cloud minimizes errors in local impingement rates on cylinders that could be attributed to a nonuniform cloud ahead of the cylinder. The reproducibility of the uniform portion of the spray cloud from one grid exposure to the next was of the order of ±3 percent variation in dye collected (based on average of two grid exposures). Variations of the cloud with respect to reproducibility were attributed to fluctuations in nozzle discharge patterns and in tunnel air flow.

The uniformity of the droplet size distribution at various locations in the cloud, was established by placing a 2-inch-diameter cylinder in three random positions in the cloud. The local impingement rates $\overline{W}_\beta$ for the cylinder at these positions were substantially identical; consequently it is reasonable to assume that the local droplet size distribution over the entire cloud was similar.

Dissolution of dye from absorbent material. - Before dissolving the dye from the blotter paper for colorimetric processing, the 1/8- by $1\frac{1}{2}$-inch ribbons from the grid were accurately trimmed to 3/4 inch in order to eliminate any end effects caused by the masking tape. The punch used to obtain the 1/8- by $1\frac{1}{2}$-inch ribbon blotters was used to remove segments from the cylinder blotters for local dye-impingement determinations. No trimming of these cylinder blotter segments was required because the punched segments are sufficiently inboard from any possible edge effects. A typical cylinder blotter with punched segments removed is shown in figure 12. The punched blotter segments were placed in individual 15 milliliter capacity test tubes and the dye dissolved out of each segment by adding a known amount of distilled water sufficient to completely cover the blotter segment (generally 5 ml). The dissolution of dye from the blotters was expedited by placing the test tube containing the distilled water and the dyed blotter segment in a water bath and heating for about 10 minutes at a temperature slightly below the boiling point. Mechanical agitation of the test tube was not employed, since agitation would promote excessive disintegration of the blotter paper. The test tubes were each covered with a vented cork to prevent the loss of a significant volume of water during heating. After heating was completed, the dye-water solutions were allowed to cool to room temperature and the effective concentration of the dye solution was determined colorimetrically. It was ascertained from successive dilutions of the same blotter segment that the initial dilution dissolved into solution more than 99 percent of the dye contained in the segment; therefore, one dilution was considered adequate.

Colorimetric analysis. - After the effective concentration of the solution in each test tube was determined from the colorimeter, a correction was made because the solution in each test tube contained a small amount of blotter fiber in suspension. These fibers absorbed some of the light in the colorimeter, causing more total light to be absorbed by the contents of the cell than would be absorbed if only a pure solution (no fibers) were analyzed. The true solution concentration P is the effective concentration of the solution minus the effective concentration of a "clean-blotter" solution. A clean blotter solution is one which contains the same amount of water as the other solutions, but the blotter segment therein has no dye on it. Since the amount of blotter

fiber in suspension appeared to be a function of the heating time, several clean blotter solutions were heated along with each batch of test tubes. An average of the effective concentrations of these clean blotter solutions was considered to be the best correction for that particular batch. Each batch consisted of all the solutions obtained from one cylinder blotter (19 from the blotter shown in fig. 12).

The amount $\bar{M}_\beta$ of dye impinging on any blotter segment per hour per square foot is given by:

$$\bar{M}_\beta \text{ (lb/(hr)(sq ft))} = \frac{Pb}{\frac{t}{3600}\Delta A_s \, 4.536\times10^5} = 7.94\times10^{-3}\frac{Pb}{t\Delta A_s} \qquad (17)$$

The weight of water (which is approximately the weight of solution) per unit weight of dye is a function of the concentration c, the percent by weight of the original dye-water solution placed in the spray system, so that

$$\frac{\bar{M}_\beta \, 100}{\bar{W}_\beta} = c \qquad (18)$$

Equations (17) and (18) result in

$$\bar{W}_\beta \text{ (lb/(hr)(sq ft))} = \frac{0.794\ Pb}{t\Delta A_s c} \qquad (19)$$

The local water impingement rates given by equation (19) are the primary results obtained by the dye-tracer techniques and are believed to be accurate and reliable (see RESULTS and DISCUSSION sections). However, the correlation of the experimental impingement characteristics obtained from these $\bar{W}_\beta$ values with the independent parameters (K, φ, etc.) requires an accurate knowledge of the droplet size distribution. Because of the inadequacies of presently available instruments for determining droplet size distribution, a method has been developed by which the droplet size distribution can be ascertained. This method, which is presented in the following section, permits the calculation of the droplet size distribution by relating the experimentally obtained $\bar{W}_\beta$ values for a body to the theoretical trajectory results for the same body.

METHOD FOR DETERMINING DROPLET SIZE DISTRIBUTION

The generalized dependent impingement parameters discussed in the section entitled BASIC IMPINGEMENT RELATIONS for both uniform droplet

size and nonuniform droplet size distributions are simplified for the cylinders used herein because the cylinders are symmetrical and are two-dimensional bodies. The resultant equations for a cylinder are:

$$E_m = \frac{y_{0,m}}{R} = \frac{1}{R} \int_{s=0}^{s=s_m} \beta \, ds \tag{20}$$

$$W_m = 0.658 \, V_0 \, w_t \, RE_m \tag{21}$$

$$\beta = \lim_{\Delta s \to 0} \frac{\Delta y_0}{\Delta s} = \frac{dy_0}{ds} \tag{22}$$

The surface distance s on a cylinder is measured from the stagnation point and may also be denoted in terms of the central angle θ measured from the stagnation point, while the limit of impingement is denoted by θ_m.

The term β may be determined from the theoretical trajectory results for any given set of impingement conditions (K, φ) by plotting y_0/R (trajectory starting ordinate at infinity) as a function of s/R (angle of impingement, radians), as shown in figure 13 (obtained from ref. 1). The slope of this curve (see eq. (22)) at any value of s/R yields the value of β at that point. A series of curves of β (ref. 1) are shown in figure 14 plotted as a function of θ for several sets of impingement conditions (combinations of K and φ). An average of the $\varphi = 1000$ group and the $\varphi = 10{,}000$ group has been cross-plotted by the use of figure 15 (from ref. 1[a]) resulting in $\beta_{[\theta, \theta_m]}$ (where β is expressed as a function of θ and θ_m) as shown in figure 16. The curves in figure 16 are essentially independent of φ for $1{,}000 \leq \varphi \leq 10{,}000$, and are required later in the analysis of the experimental impingement data.

---

[a]In obtaining figure 15 of the present report from figure 7 of reference 1, the curves of figure 7 were extrapolated to pass through $\theta_m = 0$ at $K = 1/8$. In this extrapolation, the existence of a critical value K_c of K ($K_c = 1/8$ for cylinders) was assumed. Reference 2 states that, for conditions specified by values of K less than K_c, no droplets, even those approaching along the air stagnation line, will impinge on the body; and if all impingement conditions except droplet size are specified, there is a critical droplet size a_c which will

Langmuir suggested (ref. 13, p. 4) that it might be possible to determine droplet size by comparing theoretical trajectory results for cylinders with experimental measurements of rime ice thickness on a cylinder. If theoretical trajectory results (such as those in refs. 1 and 2) were compared with $\overline{W}_\beta$ values obtained from measurements of ice thickness, the results would be of doubtful value, since the presence of the ice would change the effective contour of the cylinder and invalidate the applicability of the theoretical results. The dye-tracer method does not involve any appreciable change in cylinder contour and consequently is a more reliable source for $\overline{W}_\beta$ values. In the following method, the experimental $\overline{W}_\beta$ values for a cylinder are combined with the theoretical curves of figures 15 and 16 to determine the drop size distribution for a given set of impingement conditions (where φ is known and K is a known function of the droplet size). The basic equation which must be solved to determine the droplet size distribution is obtained by multiplying both sides of equation (14) by $0.329\ V_0\ w_t$ which, with equation (10), results in

$$\overline{W}_{\beta[\theta]} = 0.329\ V_0 \int_{w=0}^{w=w_t} \beta[\theta_m,\theta]\ dw \tag{23}$$

The subscript bracket notation indicates that $\overline{W}_\beta$ is a function of θ and that β is a function of both θ and θ_m (fig. 16). Each value of droplet radius determines a value of K for a cylinder which, with φ, specifies a value of a limit of impingement θ_m (fig. 15); hence, the problem of obtaining droplet size as a function of water content w is reduced to the problem of finding w as a function of θ_m. The

---

result in $K = K_c$. It is shown in references 2 and 3 that K_c varies with body shape, depending primarily on the flow field near the stagnation region. Because of the physical dimensions of the droplet (the droplet is considered to be a point in the theoretical analyses), the actual existence of this critical condition appears to be questionable, and no rigorous theoretical or experimental proof of the physical phenomenon occurring when $K < K_c$ has been presented. The approximate equation of motion of the droplet does change form, however, when $K = K_c$. When the accuracy of the theoretical data for small values of K is considered, it appears reasonable to extrapolate the curves to agree with the critical K concept. For the analysis presented herein, it has been assumed for simplicity that there is a critical K equal to 1/8 for cylinders. This assumption does not alter the results appreciably from those which would be obtained by assuming that θ_m approaches zero asymptotically as K approaches zero in figure 15.

exact solution of equation (23) for θ_m as a function of w is a difficult problem in the calculus of integral equations because the unknown function is neither $\overline{W}_{\beta[\theta]}$ nor $\beta[\theta_m,\theta]$. It is necessary to determine a relation between θ_m and w such that equation (23) will be satisfied for any value of θ. A method has been developed by which a close approximation to the exact mathematical solution may be obtained. The following steps describe this method, and the method is paralleled by a numerical example in appendix C:

Step 1: Divide a typical experimental $\overline{W}_\beta$ against θ curve for a cylinder (solid line, fig. 17) into arbitrary increments of θ, as shown by the vertical dotted lines in figure 17. The values of $\overline{W}_\beta$ are obtained from the dye trace on segments taken from blotters such as shown in figure 12. Also shown in figure 17 are the contributions to $\overline{W}_\beta$ of each droplet size group (dashed curves), the determination of which will be discussed in the following paragraphs.

Step 2: Assume that the unknown w against θ_m curve is composed of a block-type droplet size distribution like the dashed lines in figure 18, where each droplet size group has a θ_m equal to one of the arbitrary θ values assigned in the first step, that is,

$$\left.\begin{aligned} \theta_{m_1} = \theta_{m_{max}} &= \theta_1 \\ \theta_{m_2} &= \theta_2 \\ \cdots\cdots\cdots & \\ \theta_{m_5} &= \theta_5 \end{aligned}\right\}$$

The value of Δw for each group, however, must still be determined. Also shown in figure 18 is a solid curve representing a fairing of the block-type distribution.

Step 3: The $\overline{W}_\beta$ value obtained by analytically weighting a block-type droplet distribution curve for w against θ_m must be equal to the experimental $\overline{W}_\beta$ value at each of the chosen θ values.

The third step determines the amount Δw_1 of water contained in droplets of size a_1 specified by θ_{m_1} because all water hitting from

$\theta_2 \le \theta \le \theta_1$ (fig. 17) is made up of droplets of size specified by θ_{m_1} (condition 2, preceding). Therefore, at θ_2 where only droplets of size specified by θ_{m_1} impinge, equation (23) may be used and $\beta\left[\theta_m,\theta\right]$ becomes the constant $\beta\left[\theta_{m_1},\theta_2\right]$ and w_t is Δw_1:

$$\overline{W}_{\beta\left[\theta_2\right]} = W_{\beta\left[\theta_{m_1},\theta_2\right]} = 0.329\ V_0 \int_{w=0}^{w=\Delta w_1} \beta\left[\theta_{m_1},\theta_2\right] dw$$

$$= 0.329\ V_0\ \beta\left[\theta_{m_1},\theta_2\right] \Delta w_1$$

or

$$\Delta w_1 = \frac{W_{\beta\left[\theta_{m_1},\theta_2\right]}}{0.329\ V_0\ \beta\left[\theta_{m_1},\theta_2\right]} \tag{24}$$

Thus the magnitude of Δw_1 is determined and the values θ_{m_1} and Δw_1 describe the first droplet group, which is indicated as the bottom block in figure 18.

After the value of Δw_1 has been determined, the W_β value contributed by the first group characterized by θ_{m_1} and a_1 may be determined for all values of θ, since equation (23) shows that

$$W_{\beta\left[\theta_{m_1},\theta\right]} = 0.329\ V_0\ \Delta w_1\ \beta\left[\theta_{m_1},\theta\right] \tag{25}$$

where $\beta\left[\theta_{m_1},\theta\right]$ is determined from figure 16. $W_{\beta\left[\theta_{m_1},\theta\right]}$ can then be indicated as the height of the bottom dashed curve (curve 1) in figure 17.

The water content Δw_2 for the next droplet size group now may be determined, since for $\theta_3 \le \theta < \theta_2$ only droplets of group (1) and group (2) hit. At $\theta = \theta_3$ the amount of $\overline{W}_\beta$ due to group (1) has already been determined by equation (25). Therefore, at θ_3 the amount $W_{\beta\left[\theta_{m_2},\theta_3\right]}$ due to group (2) is

$$W_\beta\left[\theta_{m_2},\theta_3\right] = \overline{W}_\beta[\theta_3] - W_\beta\left[\theta_{m_1},\theta_3\right] \tag{26}$$

as indicated in figure 17. This value of $W_\beta\left[\theta_{m_2},\theta\right]$ determines Δw_2, since

$$\Delta w_2 = \frac{W_\beta\left[\theta_{m_2},\theta_3\right]}{0.329\ V_0\ \beta\left[\theta_{m_2},\theta_3\right]} \tag{27}$$

The value of β again is determined from figure 16 at $\theta_m = \theta_{m_2}$ and $\theta = \theta_3$. The second group may then be indicated as another block in figure 18.

The value of W_β due to the second group may be determined for all values of θ and indicated as the difference in height between dashed curves 1 and 2 in figure 17, since

$$W_\beta\left[\theta_{m_2},\theta\right] = 0.329\ V_0\ \Delta w_2\ \beta\left[\theta_{m_2},\theta\right] \tag{28}$$

where β is obtained from figure 16.

The amount of water impinging at θ_4 due to the third group may then be determined because the amounts of water contributed by the first and second groups of droplet sizes are known.

$$W_\beta\left[\theta_{m_3},\theta_4\right] = \overline{W}_\beta[\theta_4] - \left(W_\beta\left[\theta_{m_2},\theta_4\right] + W_\beta\left[\theta_{m_1},\theta_4\right]\right) \tag{29}$$

The value of Δw_3 is then determined by an equation similar to equations (24) and (27). This process is continued until a value of Δw has been determined for each droplet size group. Each group with its contribution to the total water content is indicated as a block in figure 18.

The block diagram of figure 18 is an approximation of the droplet size distribution (in terms of θ_m) to which the cylinder was exposed. This approximation is inaccurate to the extent that the weighted $\overline{W}_\beta$ (the sum of the heights between the dashed curves, fig. 17) equals the experimental $\overline{W}_\beta$ only at the selected θ points. Small increments of θ may be taken to cause the weighted $\overline{W}_\beta$ curve to approximate the

experimental $\overline{W}_\beta$ curve to any degree of accuracy desired; however, satisfactory results may be obtained by a faired curve based on only 5 or 6 increments, as shown by the solid curve in figure 18. This faired curve is reasonably independent of the choice of θ increments and when it is used to weight W_β, as described in a previous section of this report, a very close approximation to the experimental $\overline{W}_\beta$ curve is obtained.

DETERMINATION OF CLOUD LIQUID-WATER CONTENT

As previously discussed, the data from the solid curve of figure 18 may be replotted in terms of droplet radius and cumulative liquid-water content as shown in figure 19. The droplet size distribution curve in figure 19 is defined only for droplet sizes larger than a_c; the value of a_c depends on the diameter of the cylinder used. Completion of the droplet-size distribution curve through the use of progressively smaller cylinders (with accompanying smaller a_c values) is indicated. This procedure would define a greater portion of the droplet size distribution and also result in a value of w at a_c which would approach the total liquid-water content of the cloud w_t. Because it is impractical to obtain local water impingement rates on very small cylinders with the dye-tracer technique, the total liquid-water content w_t was obtained by a simple aspirating device. Details of this device and its use in obtaining the total liquid-water content are presented in appendix B.

RESULTS

The experimental data are presented in terms of local rates of water impingement $\overline{W}_\beta$ as a function of cylinder central angle θ. These data were analyzed to obtain the droplet size distribution of the impinging cloud by use of the method outlined in a previous section.

Local impingement rates and impingement limits. - The local impingement rates $\overline{W}_\beta$ for the three cylinders as determined from the dye traces by use of equation (19) are shown in figure 20 as a function of the cylinder central angle θ for three air-water pressure ratio settings of the spray nozzles. It is apparent from this figure that for a given droplet size distribution (fixed air-water pressure ratio), the smallest cylinder yields the highest local impingement rates. The local impingement rate for each cylinder also increases with increasing droplet size (as indicated by the decreasing air-water pressure ratios).

The limits of impingement ($\overline{W}_\beta = 0$) on the cylinders for the spray conditions studied are also shown in figure 20. It is apparent that as the cylinder size is decreased, the impingement on a cylinder occurs over a greater cylinder central angle θ. The average limit of impingement for three repeat runs as defined by the central angle $\theta_{m_{max}}$ varies with the air-water pressure ratio. For the 6-inch cylinder the limit of impingement changes from 46° to 74° for a change in air-water pressure ratio from 0.8 to 0.5. Comparable values for the 2-inch cylinder are 70° and 84°.

Maximum droplet size. - The maximum droplet size is determined from the experimental impingement limit ($\overline{W}_\beta \rightarrow 0$, fig. 20) by the relation of θ_m, K, and φ shown in figure 15. With φ and θ_m known, the droplet size can be readily calculated from the K parameter. Although the maximum droplet size obtained from different cylinder sizes at the same spray condition varies slightly (the smallest cylinder yields a somewhat larger droplet size value than the largest cylinder), droplet size differences are well within the range where the experimental impingement limit can be determined. At large values of θ_m, the slopes of the theoretical K against θ_m curves (fig. 15) indicate large changes in K for only small changes in θ_m; hence, a small error in θ_m will magnify the error in K or droplet size. In general, therefore, the maximum droplet size should be specified by cylinders having the maximum angles of impingement in a range where the slope of the K against θ_m curve is steep (i.e., the maximum droplet sizes determined by the largest cylinders used herein are more reliable than those determined by the smallest cylinder). The maximum droplet sizes, based on reference 1, as a function of the air-water pressure ratio are summarized as follows:

Air-water pressure ratio	Maximum droplet radius, a, microns (average for 3 repeats on 6 in. cylinder)
0.5	28.0
.6	20.4
.8	11.9

An analysis using the K against θ_m curves of reference 2 indicates a maximum droplet size approximately 15 percent greater than that obtained with the data of reference 1; however, this percentage difference in droplet size is generally in accord with the differences existing between these two theoretical studies.

Droplet size distribution and total liquid-water content. - The cumulative liquid-water content contained in the spray cloud may be determined as a function of droplet size from the results of figure 20 by the procedures discussed in the section METHOD FOR DETERMINING DROPLET SIZE DISTRIBUTION. A detailed example of the numerical procedures is given in appendix C. The curves of cumulative liquid-water content w as a function of droplet radius a based on the theoretical curves of figures 15 and 16 (ref. 1) for all three cylinders are shown in figure 21 for air-water pressure ratios of 0.5, 0.6, and 0.8. In figure 21, in the large droplet size range, the scatter among the results from the three different cylinder sizes at a constant spray condition is of the same order as the scatter between repeat runs of the same cylinders. For small droplet sizes the separation of the results relative to cylinder size (hereinafter referred to as "cylinder-size trend") is quite evident. This cylinder-size trend should not exist since, at constant spray conditions, the cloud has one droplet size distribution. Similar w against a curves are shown in figure 22 based on the theoretical data of reference 2. In general, these curves (fig. 22) are in agreement with those obtained using reference 1 (fig. 21); however, the droplet sizes are slightly larger and the cylinder-size trend in the small droplet size region is not so apparent. The differences noted (between figs. 21 and 22) are again caused by the differences inherent in the theoretical results of references 1 and 2. Because more data points are presented and the accuracy of the data is stated, reference 1 will be used hereinafter rather than reference 2 as a basis for the subsequent results.

In obtaining a single curve which is the best representation of the actual droplet size distribution existing in the tunnel for a given set of spray conditions, it is reasonable to use an average of the nine curves (three repeats times three cylinder sizes) in the larger droplet size range where the results from all three cylinder sizes are in reasonable agreement. In the range of the smaller droplet sizes ($a < 6$ microns, see fig. 21), it appears that the theoretical data are not strictly applicable because a different droplet size distribution curve is obtained for each cylinder size. However, the end point of the droplet size distribution curve ($a = 0$, $w = w_t$) is single-valued and is specified by the w_t values obtained with the aspirating device. The averages (for several repeats) of the total liquid-water content w_t obtained with the aspirator are summarized as follows:

Air-water pressure ratio	Liquid-water content, w_t g/cu m
0.5	0.70
.6	.58
.8	.43

Because of the cylinder-size trend for droplet radii less than approximately 6 microns (fig. 21), a straight line was faired between $a \approx 6$ microns and the tabulated value of w_t for each pressure ratio. The results of this interpretation of the data are shown in figure 23; the reasoning underlying this interpretation is presented in the DISCUSSION section.

Volume median droplet size and dimensionless distribution curves. - One of the more useful impingement parameters in correlating droplet size data is the volume median droplet size (ref. 2). For the three pressure ratios given, the following volume-median droplet sizes are obtained from figure 23:

Air-water pressure ratio	Volume median droplet radius, a, microns
0.5	7.4
.6	6.0
.8	3.8

Droplet size distributions are often plotted in terms of the dimensionless ratio of droplet size to the volume-median droplet size a/a_{med} as a function of percent cumulative volume of water in the cloud. A plot of a/a_{med} as a function of the percent cumulative volume $n = w/w_t$ for the three air-water pressure ratios is shown in figure 24. Although the experimental curves are not identical, the deviations are believed small enough to warrant the approximation that the three air-water pressure ratios used produce substantially the same dimensionless droplet size distribution.

DISCUSSION

The impingement data obtained by use of the dye-tracer technique are considered valid; however, certain discrepancies which cause deviations between the experimental results and theoretical analyses require

clarification. The apparent cylinder-size trend, shown in figure 21, should not occur for a given spray condition since all the cylinders are exposed to the same cloud. Probable reasons for the cylinder-size trend appear to be a combination of (1) the effect on droplet drag of droplet acceleration (ref. 14) and (2) the difference between the flow field about a cylinder assumed in references 1 and 2 (ideal fluid flow) and the flow field existing in the experimental studies. (Refs. 1 and 2 assume that the drag coefficient is a function of only the relative Reynolds number; however, reference 14 shows that the drag coefficient is also a function of the rate of change of the relative Reynolds number.) The effect on droplet drag of droplet acceleration in the flow field is to increase the drag coefficient, resulting in reduced local impingement rates, total collection efficiencies, and limits of impingement. This effect will vary with body size because a droplet experiences the acceleration for a longer time while in the flow field caused by a large body; hence, the effects may be greater for large bodies than small bodies. The effect of acceleration drag should also be less noticeable for large droplets which are not accelerated so much as small droplets. Consequently, acceleration drag would tend to produce a cylinder-size trend shown in figure 21.

A comparison of the theoretical and experimental surface velocities on cylinders is shown in figure 25. It is apparent that the local velocity ratios differ over the entire cylinder surface. The early separation of the flow (θ = approximately 50°) and the deviation of velocity ratio from the theoretical values ($\theta < 50^{\circ}$) are typical of bluff bodies studied in other wind tunnels (ref. 15). The difference between experiment and theory is due to the presence of a bluff body in a nonideal fluid and is possibly magnified by the tunnel air-stream turbulence level. These considerations indicate that such large differences in local velocity on the cylinder may mean that the flow field ahead of the cylinder is also considerably different from the theoretical flow field. Consequently, the actual droplet trajectories may be different from the theoretical calculations of reference 1 and may contribute to the cylinder-size trend shown in figure 21. In view of the possible effects of acceleration drag and flow field deviations, the agreement of the experimental data shown in figure 21 appears reasonable.

Additional factors that have been considered to account for the cylinder-size trend include: droplet evaporation effects, splatter of droplets on blotter paper, effect of blotter texture on local water catch, oscillation or pulsation of spray cloud in the air stream, initial relative velocity differences between droplet and air, droplet distortion effects on droplet drag coefficient, boundary layer considerations, and accuracy (with regard to the mechanics of the analyzer) of the theoretical trajectories (ref. 1). Evaluations of the effect of these factors on the cylinder-size trend all indicated a negligible effect or an effect that would produce a minor trend opposite to that obtained in the experimental study.

As stated in the RESULTS and presented in figure 23, a straight line was assumed to define the droplet size distribution curves between droplet radii of approximately 6 and 0 microns. The extremities of this fairing appear reasonably well defined: (1) Analysis of droplet size values from all cylinders in figure 21 are in general agreement for $a > 6$ microns and (2) at a equal to zero in figure 23, the value of total liquid-water content from the aspirator is considered valid. Between droplet radii of 6 and 0 microns (see fig. 23), three general fairings are possible: (1) a straight line as shown, (2) a concave fairing, or (3) a convex fairing. The concave fairing would indicate that the cloud contains a multitude of extremely small (of the order of $a = 1$ micron) droplets and very few droplets of the order of radius 2 to 5 microns. The convex fairing, on the other hand, would indicate a large number of droplets of the order of 2 to 5 microns in radius and very few droplets less than about 2 microns in radius.

As previously shown in figure 21, the droplet size distribution curve (obtained with the theoretical trajectory data of ref. 1) approaches the concave-type fairing for droplet sizes <6 microns in radius; however, each cylinder size indicates a considerably different concave fairing of droplet distribution data for the same spray condition. This contradiction makes any fairing based on these theoretical trajectories unreliable in this droplet size range.

It should be possible to obtain values of total liquid-water content from the experimentally determined impingement rates on the grid ribbons by using the theoretical trajectory data of reference 2. If the w_t values so determined are to agree with the w_t values obtained with the aspirating device, the droplet size distribution curve (in the range of droplet sizes <6 microns in radius) would necessarily require a concave fairing. However, the theoretical trajectory results for a ribbon (ref. 2) are subject to the same limitations (such as neglecting acceleration drag etc.) which are inherent in the cylinder trajectories (ref. 1) and which are believed responsible for the cylinder-size trend shown in figure 21. The theoretical trajectory data for ribbons and cylinders therefore are not considered an adequate guide in fairing the droplet size distribution curves of figure 23 for droplet radii less than approximately 6 microns.

In the small droplet size range ($a < 6$ microns), unpublished data from oiled slides and a droplet sampler currently being developed, although subject to sampling errors due to unreliable values of collection efficiency, show no indication of a concave-type droplet size distribution. These data indicate a convex shape or possibly a straight-line fairing.

In general, an abrupt lack of droplet sizes of the order of 2 to 5 microns in radius coupled with a multitude of droplets less than 1 micron

in radius appears to be improbable. On the other hand, a distribution of droplet sizes from 6 microns in radius down to some finite but limiting size such as 1 or 2 microns in radius (convex distribution) appears feasible with an air-atomizing nozzle of the type used herein.

Because all available evidence supporting the concave-type fairing for the range of droplet radii less than approximately 6 microns in figure 23 appears contradictory and because the experimental evidence supporting the convex fairing is insufficient to determine the extent to which the curve should be convex, the straight-line (dashed) fairing of figure 23 is used.

The accuracy of determining droplet size distribution by the use of the dye-tracer technique together with theoretical trajectory data could be definitely established if an accurate instrument were available to measure directly a representative sample of all droplet sizes present in the experimental spray cloud. The present state of development of the camera (ref. 16) or the oiled-slide technique (ref. 17) for measuring droplet size is not considered so adequate a means for determining droplet size as the indirect method herein described.

CONCLUDING REMARKS

A technique for experimentally determining the impingement characteristics of an arbitrary body and a method whereby the droplet size spectrum of the spray cloud can be determined from the experimental impingement on a body for which the theoretical trajectories are known have been developed. These developments present an opportunity to study experimentally the impingement characteristics of other shapes such as airfoils, radomes, inlet cowlings, and asymmetrical bodies. Although analytical trajectory studies can be made for these various bodies, the problems associated with the determination of the flow fields and consequent droplet trajectories often prove difficult and tedious. Use of the dye-tracer technique for arbitrary shapes in any suitable testing facility would proceed as described herein for cylinders: The droplet size distribution in the spray cloud would be established using bodies for which the theoretical impingement characteristics are known, while an aspirating device similar to the one described (appendix B) may be used for the determination of total liquid-water content. The unknown body with blotter then would be exposed and analyzed for local rates of water impingement, including the determination of the maximum extent or limit of impingement, and integrated for total collection efficiency.

Impingement limits and collection efficiency are often presented in terms of K and φ (where K is indicative of the inertia of the droplet and φ represents the deviation of the drag forces from Stokes' law) for correlating impingement characteristics. Langmuir has suggested

the use of a modified K parameter. Reference 18 discusses and illustrates previous analytically determined impingement data (for cylinders, airfoils, ribbons, spheres) in terms of a K_0 parameter ($K_0 = (\lambda/\lambda_s)\,K$) where λ is the true range a droplet would have when projected into still air and λ_s is the range of a droplet obeying Stokes law. Plotting a dependent impingement parameter, such as total collection efficiency, as a function of K_0 yields an essentially single-valued curve (for most of the simple bodies for which trajectory results are presently available) independent of φ, this curve being the Stokes' law solution. The extension or interpolation of experimental as well as analytical data points over a wide range of the pertinent impingement variables - droplet size, body size, speed, and altitude - is greatly facilitated by this K_0 parameter, even though no rigorous theoretical proof of the significance of K_0 is available at this time.

The dimensionless impingement parameters previously discussed (K, φ, ψ, Re_0, and K_0) are presented in the literature in terms of clouds containing droplets of the same size. Analytical calculations have shown that the presence of a droplet size distribution does not alter the usefulness of the K_0 parameter if it is evaluated with a pertinent cloud characteristic. Using volume-median or -maximum droplet size of the distribution to calculate K_0 will tend to reduce total collection efficiency or limit of impingement, respectively, to single-valued curves (Stokes' law solutions). The total collection efficiency curve as a function of $(K_0)_{med}$ for a droplet size distribution will be somewhat skewed from that obtained with a uniform droplet size spectrum; the amount of skew depends on the droplet size distribution. Reasonable extension and interpolation of experimental data for conditions other than those studied is possible with the K_0 parameter.

Further analysis has shown that the dependent impingement parameters for the case of uniform droplet size (such as obtained from trajectory results) may be obtained from a series of experimental impingement rate curves ($\overline{W}_\beta$ against s/L) when the experimental droplet size distribution is known. The method requires curves of $\overline{W}_\beta$ against s/L, which may be obtained by the dye-tracer technique for either (1) one body in the presence of several (say about six) different, but known, droplet distributions or (2) several sizes of the body in the presence of one droplet distribution. The method of calculation is a step-wise approximation and may be derived by methods similar to those used for obtaining the droplet distribution in the section METHOD OF DETERMINING DROPLET-SIZE DISTRIBUTION. The results of such an analysis would be useful in (1) calculating the impingement rates for a body in a cloud of arbitrary

droplet size distribution, and (2) determining whether the assumptions used in theoretical trajectory calculations are valid. This determination requires an independent means (reliable instrument) for measuring the droplet size distribution.

Lewis Flight Propulsion Laboratory
National Advisory Committee for Aeronautics
Cleveland, Ohio, November 3, 1954

APPENDIX A

SYMBOLS

The following symbols are used in this report:

A area, sq ft

A_0 area (perpendicular to air stream) at $x = -\infty$, sq ft

a droplet radius, microns (3.281×10^{-6} ft)

b volume of water used to dissolve dye from blotter segments, ml

c percent concentration by weight of dye in water solution used in spray system $\frac{\text{lb dye}}{\text{lb solution}} \times 100 \text{ percent} \cong \frac{\text{lb dye}}{\text{lb water}} \times 100 \text{ percent}$

E_m total collection efficiency in clouds of uniform droplet size defined by eq. (1), dimensionless

K inertia parameter, $\frac{2.19 \times 10^{-10} \, a^2 V_0}{\mu L}$, dimensionless

K_0 modified inertia parameter, $\frac{\lambda}{\lambda_s} K$, dimensionless

L a significant body dimension: chord length of airfoil, radius of cylinder, one-half ribbon width, ft

$\bar{M}_\beta$ local dye collection rate, lb/(hr)(sq ft)

n cumulative fraction of total liquid-water content = w/w_t, dimensionless

P true concentration of solution obtained from blotter segments, $\frac{\text{mg dye}}{\text{ml solution}}$

R cylinder radius, ft

Re_0 free-stream Reynolds number with respect to droplet, $\frac{9.62\times10^{-6}\ a\rho V_0}{\mu} = \sqrt{K\ \varphi}$, dimensionless

s distance along surface from point of reference, ft

t exposure time, sec

V_0 free stream velocity, mi/hr

W_m total water impingement rate in cloud of uniform droplet size, lb/(hr)

W_β local water impingement rate in cloud of uniform droplet size, lb/(hr)(sq ft)

w cumulative liquid-water content contained in droplets of sizes from a_{max} to any particular droplet size, g/cu m

w_t total liquid-water content of cloud, g/cu m

x abscissa of coordinate system parallel to free-stream velocity direction, ft (see fig. 1)

y_0 ordinate of coordinate system perpendicular to free-stream velocity direction at $x = -\infty$, ft (see fig. 1)

β local collection efficiency in cloud of uniform droplet size, defined by eq. (4), dimensionless

θ central angle of cylinder measured from x-axis, 57.3 s/R, deg

λ true range of droplet as a projectile injected into still air, ft

λ_s range of droplet as a projectile following Stokes' law, ft

μ viscosity of air, lb/(ft)(sec)

ρ density of air, lb/cu ft

φ independent impingement parameter, $\frac{0.423\ \rho^2 V_0 L}{\mu}$, dimensionless

ψ independent impingement parameter, $\frac{4.40\times10^4\ \rho L}{a}$, dimensionless

Subscripts:

c critical condition for impingement

f frontal, projected parallel to free-stream velocity direction

m tangent trajectory

med volume median

max maximum droplet size

s surface

0,1, 2,3,n particular values of a variable

[ ] brackets denote functional notation

Superscript:

– weighted value due to effects of more than one droplet size

APPENDIX B

DESCRIPTION OF ASPIRATING DEVICE

An aspirating device was used to obtain measurements of the total liquid-water content of the cloud. This device consisted essentially of a tube which sucked in the approaching air and cloud droplets at the free-stream velocity (inlet velocity ratio, 1.0) so that both the air streamlines and droplets entered the tube along straight-line paths. All the dyed droplets were deposited on a filter mounted within the tube, leaving a dye trace which could be analyzed colorimetrically.

The inlet tube consisted of stainless steel tubing (10- by 1/4-in. O.D. by 0.014-in. wall thickness) with the front end tapered to the internal diameter. Behind the inlet tube was a diffuser section increasing in I.D. to 3/4 inch. The increase in cross-sectional area decreased the velocity through the diffuser, and consequently reduced the pressure drop in the following section where the filters were mounted. The filters consisted of small circular cloth pads spaced about 1/16 inch apart axially. A sufficient number of filters were used so that after exposure the rearmost filter was always free of dye, indicating that no dye passed downstream of the filter section. Air flow through the aspirating device was obtained by the use of an ejector attached aft of the filter section with an exhaust line. The suction in this exhaust line could be regulated to adjust the weight flow through the tube. The pressure was measured with a static tap on the inside of the inlet tube 3/4 inch from the front end. The tap had been calibrated to give pressure as a function of the weight flow through the tube and was used as an indicator for obtaining a weight flow equivalent to an inlet velocity ratio of 1.0. The device was mounted in the tunnel with the inlet tube parallel to and facing into the air stream. The suction in the exhaust line was adjusted to obtain the correct inlet velocity ratio, and then the device was exposed to the spray cloud in the same manner as for the cylinder models. After exposure, the filters were removed, and the dye in the filters along with any dye left on the inside of the inlet tube and diffuser was dissolved into a known quantity of water. The concentration of the resulting solution was measured colorimetrically.

Equation (19) was modified to evaluate the rate of water catch for the aspirating device as follows:

$$\overline{W}_{\beta}^{*} = \frac{0.794\ F^{*} b^{*}}{tc\ \Delta A_{s}^{*}}$$

where

$\overline{W}_\beta^*$ total rate of water catch $\overline{W}_m$ divided by frontal area A_f of inside cross section of tube

P^* effective concentration (mg/ml); also considered true concentration because only a negligible amount of filter fibers were in the solution

b^* total amount of water (ml) used to dissolve dye from inside walls of device and filters

ΔA_s^* equal to frontal area A_f of inside cross section of tube

Because all the droplets directly ahead of the inside cross-sectional area of the tube enter the tube (straight-line trajectories), the collection efficiency $\overline{E}_m$ of the aspirating device is 1.0, and the $\overline{W}_\beta^*$ value may be used in equation (9) to determine the total liquid-water content of the cloud:

$$w_t = \frac{\overline{W}_m}{0.329\ V_0 A_f \overline{E}_m} = \frac{\overline{W}_\beta^*}{0.329\ V_0 \overline{E}_m} = \frac{0.794\ P^* b^*}{0.329\ tc\ \Delta A_s^* V_0\ 1.0}$$

APPENDIX C

NUMERICAL EXAMPLE OF DETERMINATION OF DROPLET DISTRIBUTION FROM EXPERIMENTAL LOCAL WATER IMPINGEMENT RATE

The $\overline{W}_\beta$ values for this example are obtained from the repeat curve for the 2-inch cylinder in figure 20(a). For these data, $K = 0.0387a^2$ and $\varphi = 2800$.

A convenient setup for use in calculating the droplet size distribution is shown in table I. The first column represents the arbitrary values of θ at which the $\overline{W}_\beta$ curve was divided. The second column represents the corresponding values of $\overline{W}_\beta$ (i.e., $\overline{W}_{\beta[\theta_3]} = 2.99$). The top row represents the values of θ_m, each equal to a θ value and each specifying a droplet size group. In any box, determined by the intersection of a θ row and a θ_m column, the number above the diagonal line is the value β for that value of θ_m at that value of θ as determined from figure 16 (i.e., $\beta_{[\theta_{m_5},\theta_7]} = \beta_{[40^\circ,20^\circ]} = 0.335$). The number below the diagonal line in any box is the corresponding value of W_β (which is part of $\overline{W}_\beta$ at that value of θ). The object of the calculation is to determine the values of Δw in the second row. The procedure outlined in the METHOD OF ANALYSIS section gives the following results:

Group 1:

$$W_{\beta[\theta_{m_1},\theta_2]} = \overline{W}_{\beta[\theta_2]} = 0.62$$

$$\Delta w_1 = \frac{W_{\beta[\theta_{m_1},\theta_2]}}{0.329\ V_0\ \beta_{[\theta_{m_1},\theta_2]}} = \frac{0.62}{57.6(0.237)} = 0.0454 \qquad (24)$$

$$W_{\beta[\theta_{m_1},\theta]} = (57.6\ \Delta w_1)\ \beta_{[\theta_{m_1},\theta]} =$$

Beneath diagonal line in θ_{m_1} column

$$\begin{cases} = (57.6)(0.0454)(0.237) = 0.62 \text{ for } \theta_2 \\ = (57.6)(0.0454)(0.406) = 1.06 \text{ for } \theta_3 \\ \cdots\cdots\cdots\cdots\cdots\cdots \\ = (57.6)(0.0454)(0.942) = 2.46 \text{ for } \theta_9 \end{cases} \qquad (25)$$

For subsequent droplet size groups the numerator of the equation for Δw_n is the $\bar{W}_\beta$ at θ_{n+1} minus the sum of the W_β values contributed by the preceding droplet size groups in the particular θ_{n+1} row.

Group 2:

$$W_\beta\left[\theta_{m_2},\theta_3\right] = \bar{W}_\beta\left[\theta_3\right] - W_\beta\left[\theta_{m_1},\theta_3\right] = 2.99 - 1.06 = 1.93 \tag{26}$$

$$\Delta w_2 = \frac{W_\beta\left[\theta_{m_2},\theta_3\right]}{0.329\ V_0\ \beta\left[\theta_{m_2},\theta_3\right]} = \frac{1.93}{(57.6)(0.183)} = 0.183 \tag{27}$$

$$W_\beta\left[\theta_{m_2},\theta\right] = 57.6 \times \Delta w_2\ \beta\left[\theta_{m_2},\theta\right] =$$

Beneath diagonal line in θ_{m_2} column

$$\begin{cases} = 57.6\ (0.183)(0.183) = 1.93 \text{ for } \theta_3 \\ = 57.6\ (0.183)(0.344) = 3.63 \text{ for } \theta_4 \\ \cdots\cdots\cdots\cdots\cdots\cdots \\ = 57.6\ (0.183)(0.814) = 8.58 \text{ for } \theta_9 \end{cases} \tag{28}$$

Group 3:

$$W_\beta\left[\theta_{m_3},\theta_4\right] = \bar{W}_\beta\left[\theta_4\right] - \left(W_\beta\left[\theta_{m_1},\theta_4\right] + W_\beta\left[\theta_{m_2},\theta_4\right]\right)$$

$$= 6.50 - (1.45 + 3.63) = 1.42 \tag{29}$$

$$\Delta w_3 = \frac{W_\beta\left[\theta_{m_3},\theta_4\right]}{0.329\ V_0\ \beta\left[\theta_{m_3},\theta_4\right]} = \frac{1.42}{57.6(0.187)} = 0.132$$

$$W_\beta\left[\theta_{m_3},\theta\right] = 57.6\ \Delta w_3\ \beta\left[\theta_{m_3},\theta\right] =$$

Beneath diagonal line in θ_{m_3} column

$$\begin{cases} = 57.6\ (0.132)(0.187) = 1.42 \text{ for } \theta_4 \\ = 57.6\ (0.132)(0.351) = 2.66 \text{ for } \theta_5 \\ \cdots\cdots\cdots\cdots\cdots\cdots \\ = 57.6\ (0.132)(0.704) = 5.35 \text{ for } \theta_9 \end{cases}$$

Group 4:

$$W_\beta\left[\theta_{m_4},\theta_5\right] = \bar{W}_\beta\left[\theta_5\right] - \left(W_\beta\left[\theta_{m_1},\theta_5\right] + W_\beta\left[\theta_{m_2},\theta_5\right] + W_\beta\left[\theta_{m_3},\theta_5\right]\right)$$

$$= 9.78 - (1.79 + 5.32 + 2.66) = 0.01$$

$$\Delta w_4 = \frac{W_\beta\left[\theta_{m_4},\theta_5\right]}{0.329\ V_0\ \beta\left[\theta_{m_4},\theta_5\right]} = \frac{0.01}{57.6(0.183)} = 0.00095$$

and so forth. This process is continued until a value of Δw is determined for each group.

The resulting block diagram is shown by the straight solid lines in figure 26. A solid curve is faired through this block diagram. For a known value of φ, figure 15 may be used to determine K and hence a, droplet radius, as a function of θ_m. The droplet size scale thus determined is shown along with the θ_m scale in figure 26. The values of w as a function of droplet radius read from the solid curve of figure 26 are identical to those for one of the three 2-inch-cylinder curves in figure 21(c).

The significance of the θ_m increments selected for row 1 in the preceding table is illustrated by the dotted curve in figure 26, which results from dividing the $\bar{W}_\beta$ curve at θ = 83.7, 75, 65, 55, 45, 35, 25, 15, 5, and 0 degrees. The dashed and the solid curves are almost identical.

REFERENCES

1. Brun, Rinaldo J., and Mergler, Harry W.: Impingement of Water Droplets on a Cylinder in an Incompressible Flow Field and Evaluation of Rotating Multicylinder Method for Measurement of Droplet-Size Distribution, Volume-Median Droplet Size, and Liquid-Water Content in Clouds. NACA TN 2904, 1953.

2. Langmuir, Irving, and Blodgett, Katherine B.: A Mathematical Investigation of Water Droplet Trajectories. Tech. Rep. No. 5418, Air Materiel Command, AAF, Feb. 19, 1946. (Contract No. W-33-038-ac-9151 with General Electric Co.)

3. Tribus, Myron: Modern Icing Technology - Lecture Notes. Eng. Res. Inst., Univ. of Michigan, Jan. 1952. (Air Res. and Dev. Command, USAF Contract AF 18(600)-51, E.O. No. 462 Br-1, Proj. M992-E.)

4. Bergrun, Norman R.: A Method for Numerically Calculating the Area and Distribution of Water Impingement on the Leading Edge of an Airfoil in a Cloud. NACA TN 1397, 1947.

5. Brun, Rinaldo J., Gallagher, Helen M., and Vogt, Dorthea E.: Impingement of Water Droplets on NACA 65A004 Airfoil and Effect of Change in Airfoil Thickness from 12 to 4 Percent at 4° Angle of Attack. NACA TN 3047, 1953.

6. Brun, Rinaldo J., Gallagher, Helen M., and Vogt, Dorthea E.: Impingement of Water Droplets on NACA 65_1-208 and 65_1-212 Airfoil at 4° Angle of Attack. NACA TN 2952, 1953.

7. Guibert, A. G., Janssen, E., and Robbins, W. M.: Determination of Rate, Area, and Distribution of Impingement of Waterdrops on Various Airfoils from Trajectories Obtained on the Differential Analyzer. NACA RM 9A05, 1949.

8. Brun, Rinaldo J., Serafini, John S., and Gallagher, Helen M.: Impingement of Cloud Droplets on Aerodynamic Bodies as Affected by Compressibility of Air Flow Around the Body. NACA TN 2903, 1953.

9. Serafini, John S.: Impingement of Water Droplets on Wedges and Double-Wedge Airfoils at Supersonic Speeds. NACA Rep. 1159, 1954. (Supersedes NACA TN 2971.)

10. Brun, Rinaldo J., and Dorsch, Robert G.: Impingement of Water Droplets on an Ellipsoid with Fineness Ratio 10 in Axisymmetric Flow. NACA TN 3147, 1954.

11. Dorsch, Robert G., Brun, Rinaldo J., and Gregg, John L.: Impingement of Water Droplets on an Ellipsoid with Fineness Ratio 5 in Axisymmetric Flow. NACA TN 3099, 1954.

12. Bergrun, Norman R.: An Emperical Method Permitting Rapid Determination of the Area, Rate, and Distribution of Water-Drop Impingement on an Airfoil of Arbitrary Section at Subsonic Speeds. NACA TN 2476, 1951.

13. Langmuir, Irving: Super-Cooled Water Droplets in Rising Currents of Cold Saturated Air, Pt. I. Res. Lab., General Electric Co., Oct. 1943-Aug. 1944. (Army Contract W-33-106-sc-65.)

14. Hughes, R. R., and Gilliland, E. R.: The Mechanics of Drops. Proc. Heat Transfer and Fluid Mech. Inst., 1951, pp. 53-72.

15. Giedt, W. H.: Effect of Turbulence Level of Incident Air Stream on Local Heat Transfer and Skin Friction on a Cylinder. Jour. Aero. Sci., vol. 18, no. 11, Nov. 1951, pp. 725-730; 766.

16. McCullough, Stuart, and Perkins, Porter J.: Flight Camera for Photographing Cloud Droplets in Natural Suspension in the Atmosphere. NACA RM E50K01a, 1951.

17. Golitzine, N.: Method for Measuring the Size of Water Droplets in Clouds, Fogs, and Sprays. Note 6, Nat. Aero. Est. (Canada), 1951.

18. Sherman, P., Klein, J. S., and Tribus, M.: Determination of Drop Trajectories by Means of an Extension of Stokes' Law. Eng. Res. Inst., Air Res. and Dev. Command, USAF, Univ. Mich., Apr. 1952. (Contract AF 18(600)-51, Proj. M992-D.)

TABLE I. - SETUP FOR CALCULATING DROPLET SIZE DISTRIBUTION FROM CYLINDER IMPINGEMENT

		Group 1	Group 2	Group 3	Group 4	Group 5	Group 6	Group 7	Group 8	Group 9
	θ_m →	$\theta_{m_1} = 83.7$	$\theta_{m_2} = 70$	$\theta_{m_3} = 60$	$\theta_{m_4} = 50$	$\theta_{m_5} = 40$	$\theta_{m_6} = 30$	$\theta_{m_7} = 20$	$\theta_{m_8} = 10$	$\theta_{m_9} = 0$
	Δw →	$\Delta w_1 = 0.0454$	$\Delta w_2 = 0.183$	$\Delta w_3 = 0.132$	$\Delta w_4 = 0.00095$	$\Delta w_5 = 0.00963$	$\Delta w_6 = 0.0302$	$\Delta w_7 = 0.0049$	$\Delta w_8 = 0.0168$	$\Delta w_9 = 0$
θ ↓	$\overline{W}\beta[\theta]$ ↓	$\beta[\theta_{m_1},\theta]$ / $W_\beta[\theta_{m_1},\theta]$	$\beta[\theta_{m_2},\theta]$ / $W_\beta[\theta_{m_2},\theta]$	$\beta[\theta_{m_3},\theta]$ / $W_\beta[\theta_{m_3},\theta]$	$\beta[\theta_{m_4},\theta]$ / $W_\beta[\theta_{m_4},\theta]$	$\beta[\theta_{m_5},\theta]$ / $W_\beta[\theta_{m_5},\theta]$	$\beta[\theta_{m_6},\theta]$ / $W_\beta[\theta_{m_6},\theta]$	$\beta[\theta_{m_7},\theta]$ / $W_\beta[\theta_{m_7},\theta]$	$\beta[\theta_{m_8},\theta]$ / $W_\beta[\theta_{m_8},\theta]$	$\beta[\theta_{m_9},\theta]$ / $W_\beta[\theta_{m_9},\theta]$
$\theta_1 = 83.7$	0	0 / 0								
$\theta_2 = 70$	0.62	0.237 / 0.62	0 / 0							
$\theta_3 = 60$	2.99	0.406 / 1.06	0.183 / 1.93	0 / 0						
$\theta_4 = 50$	6.50	0.553 / 1.45	0.344 / 3.63	0.187 / 1.42	0 / 0					
$\theta_5 = 40$	9.78	0.685 / 1.79	0.504 / 5.32	0.351 / 2.66	0.183 / 0.01	0 / 0				
$\theta_6 = 30$	12.69	0.792 / 2.07	0.635 / 6.70	0.500 / 3.80	0.345 / 0.019	0.182 / 0.101	0 / 0			
$\theta_7 = 20$	15.16	0.873 / 2.28	0.731 / 7.71	0.611 / 4.64	0.477 / 0.026	0.335 / 0.186	0.183 / 0.318	0 / 0		
$\theta_8 = 10$	16.81	0.922 / 2.41	0.792 / 8.35	0.681 / 5.71	0.563 / 0.031	0.442 / 0.245	0.318 / 0.553	0.181 / 0.051	0 / 0	
$\theta_9 = 0$	17.55	0.942 / 2.46	0.814 / 8.58	0.704 / 5.35	0.590 / 0.032	0.480 / 0.266	0.370 / 0.643	0.261 / 0.074	0.150 / 0.145	0 / 0

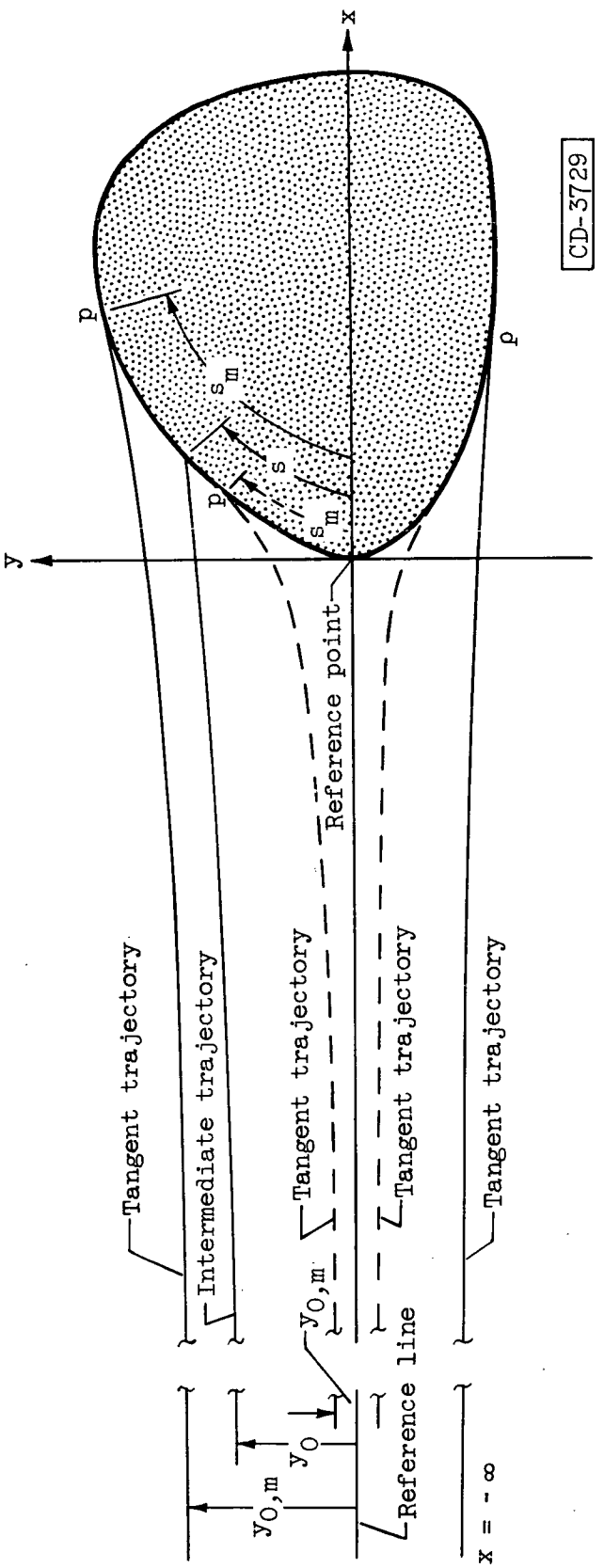

Figure 1. - Typical trajectories for simple two-dimensional body. Momentum effect of droplets is greater for solid trajectories than for dashed ones.

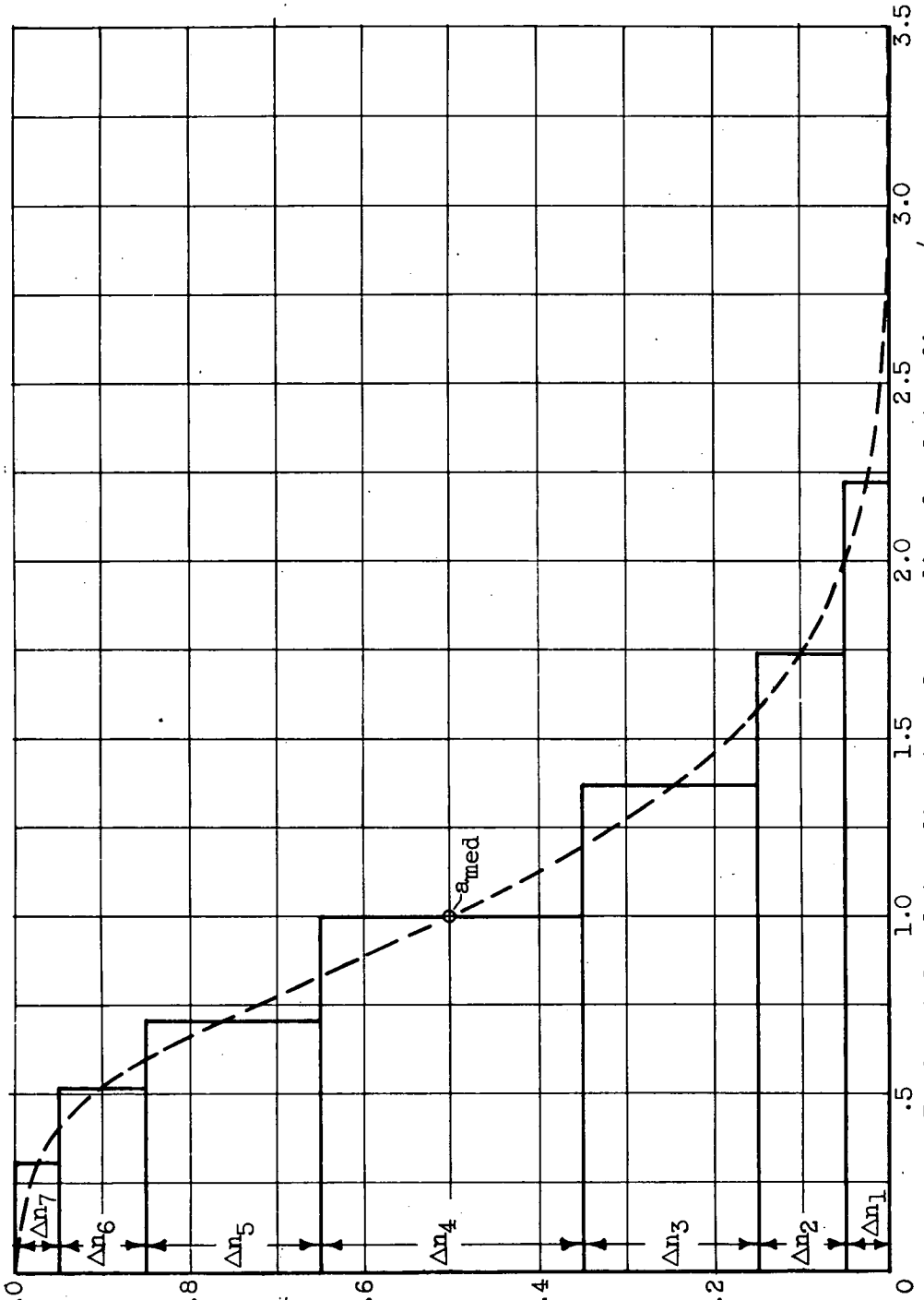

Figure 2. - Hypothetical dimensionless distribution of droplet sizes. Langmuir D-type distribution from reference 2.

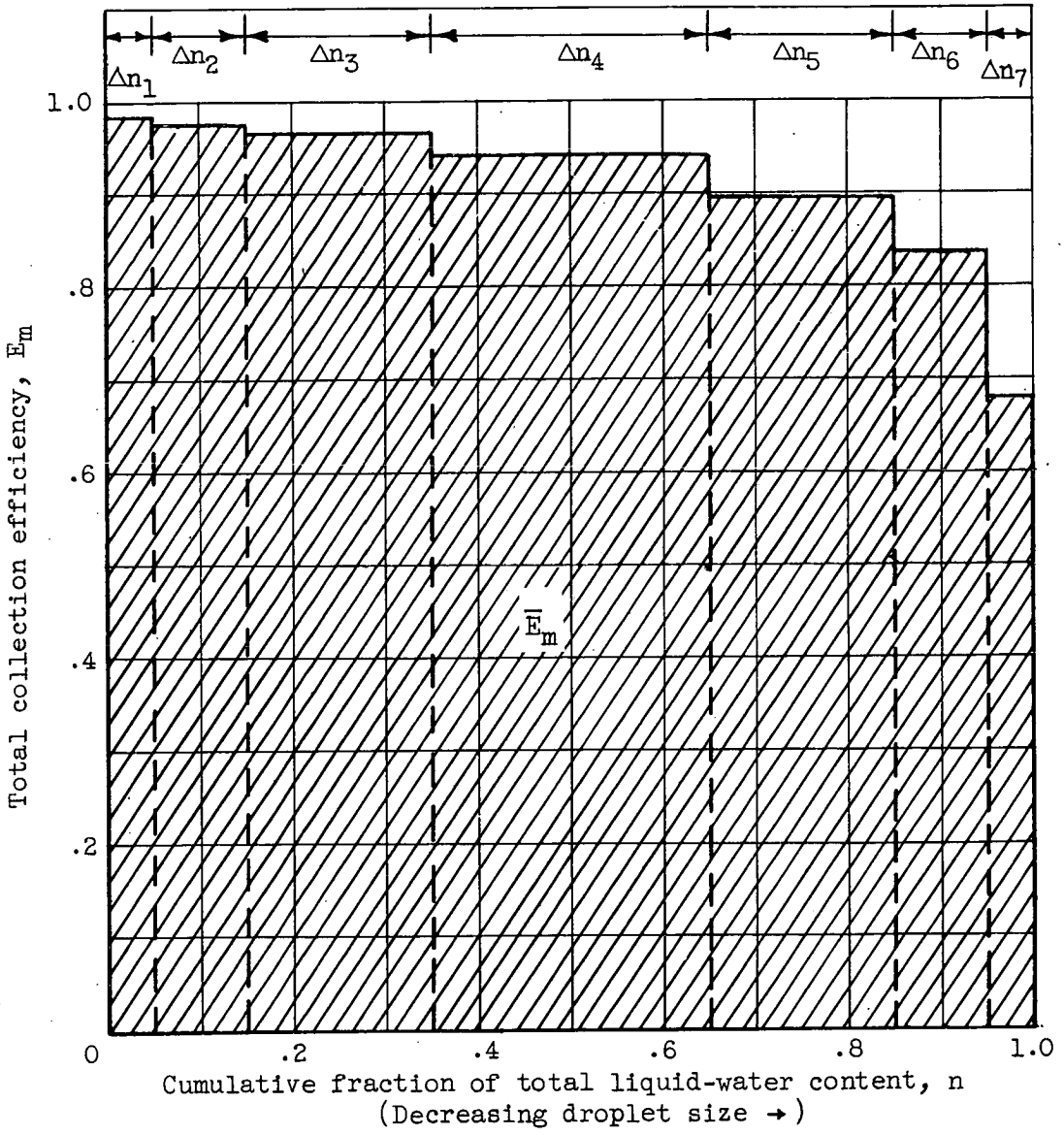

(a) Block-type droplet distribution.

Figure 3. - Typical representation of weighted total collection efficiency $\bar{E}_m$ as summation of contributions by each droplet size in distribution. Cross-hatched area equals $\bar{E}_m$.

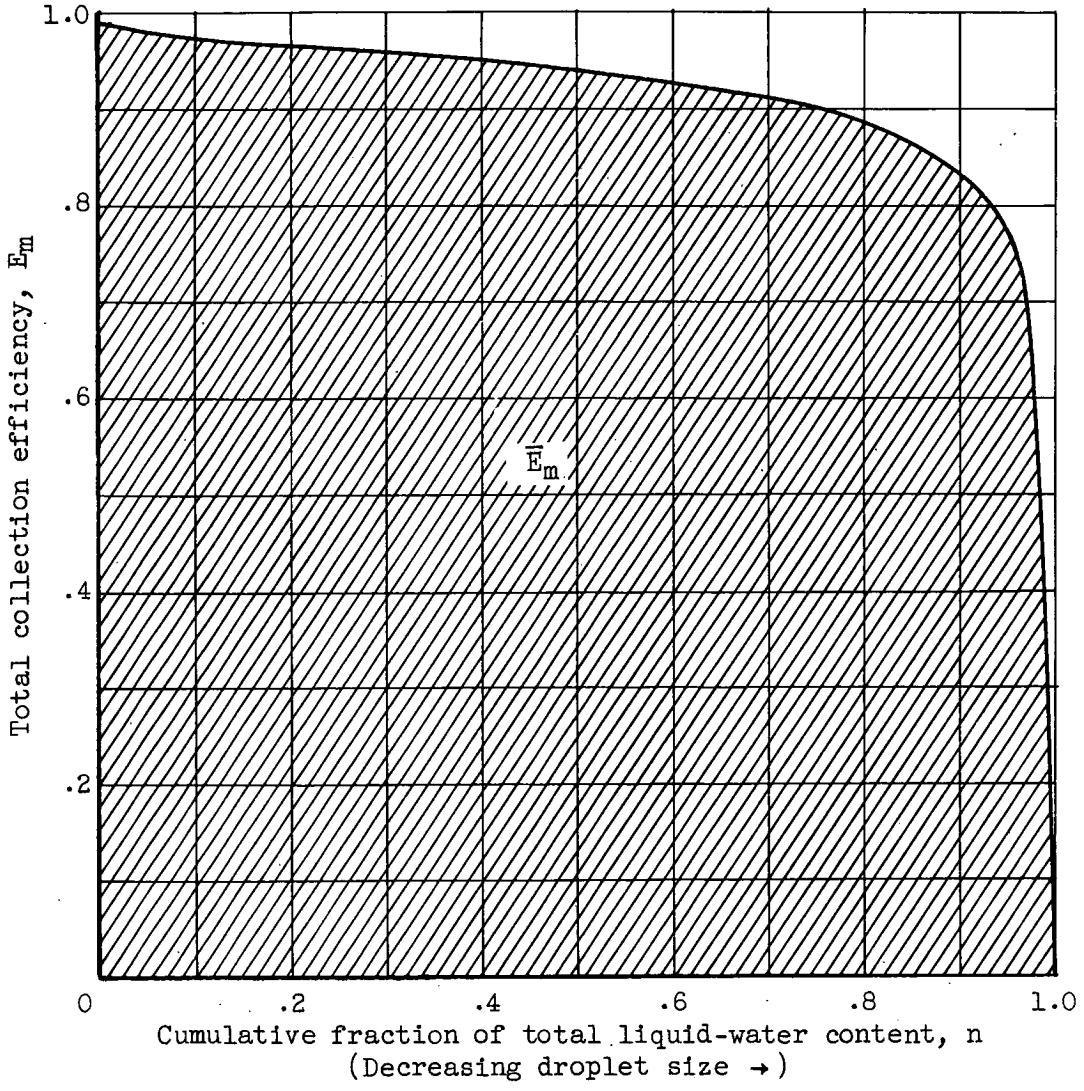

(b) Faired-type droplet distribution.

Figure 3. - Concluded. Typical representation of weighted total collection efficiency $\bar{E}_m$ as summation of contributions by each droplet size in distribution. Cross-hatched area equals $\bar{E}_m$.

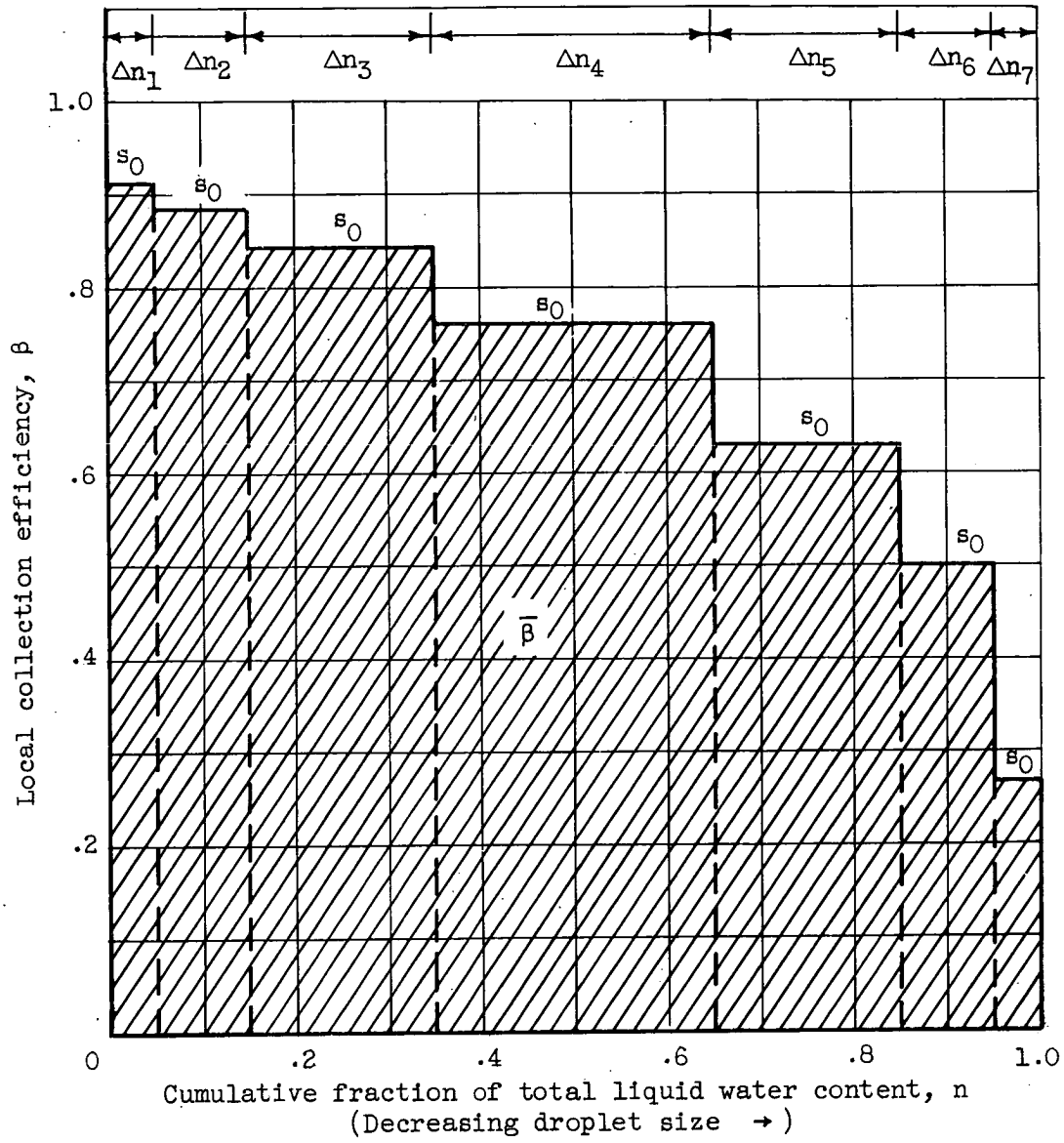

Figure 4. - Typical representation of weighted local collection efficiency $\bar{\beta}$ as summation of contributions by each droplet-size group in distribution for one particular surface location s_0 on two-dimensional body for block-type droplet distribution. Cross-hatched area represents $\bar{\beta}$ at s_0.

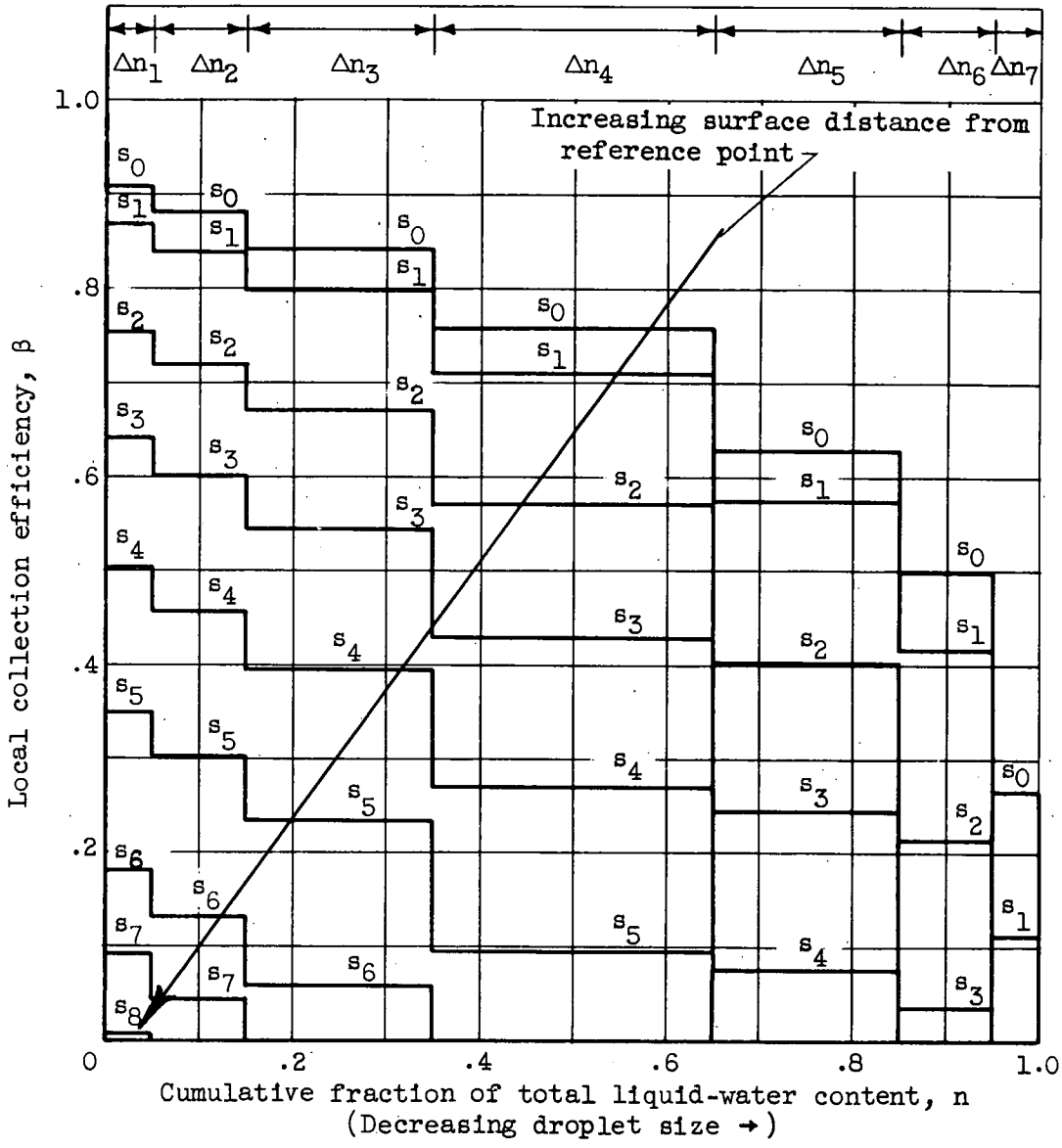

Figure 5. - Typical variation of weighted local collection efficiency $\bar{\beta}$ (represented by area under a particular s_n curve) as function of surface location on two-dimensional body for block-type droplet distribution.

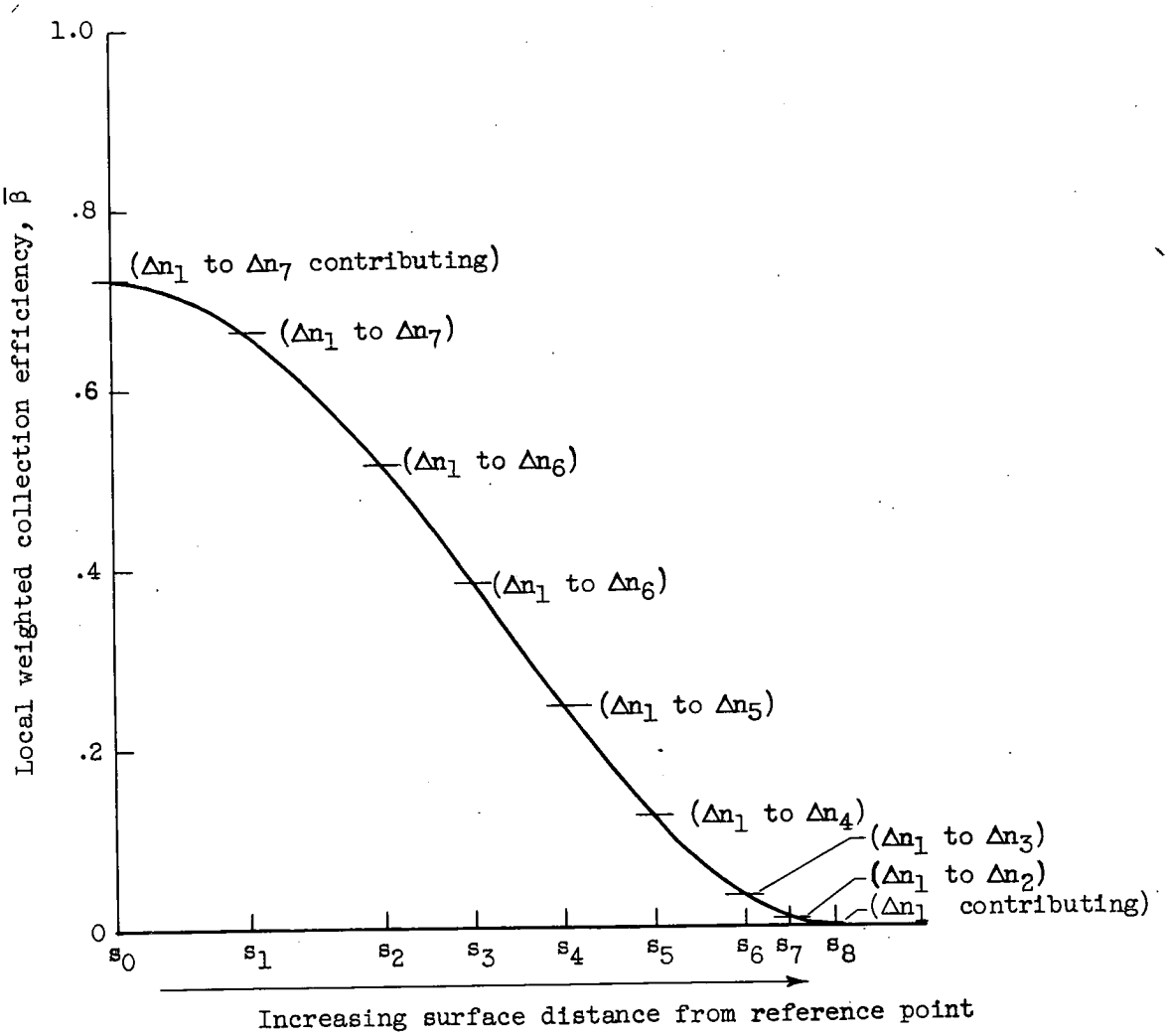

Figure 6. - Typical variation of weighted local collection efficiency $\bar{\beta}$ as function of surface location on two-dimensional body for block-type droplet distribution.

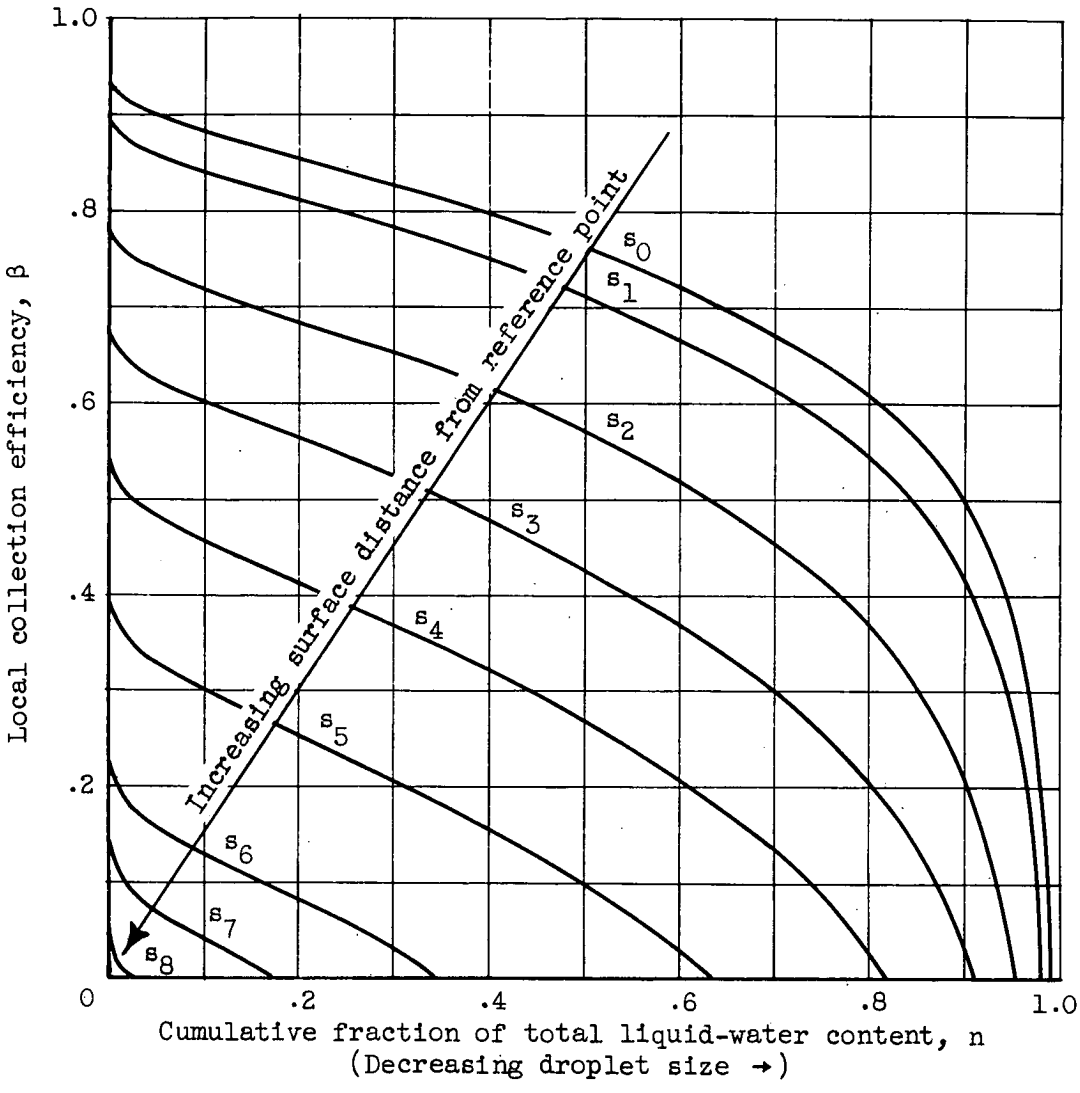

Figure 7. - Typical variation of weighted local collection efficiency $\bar{\beta}$ (represented by area under particular s_n curve) as function of surface location on two-dimensional body for faired-type droplet distribution.

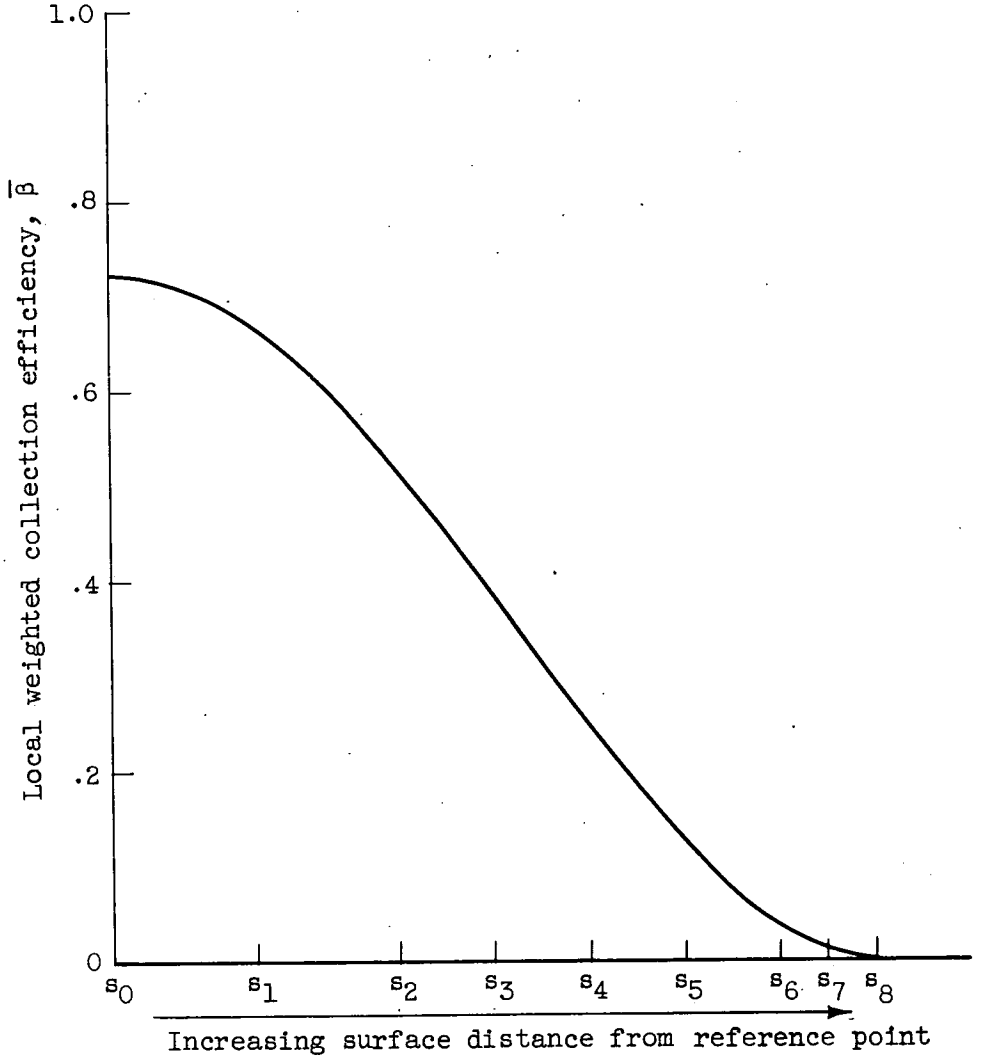

Figure 8. - Typical variation of weighted local collection efficiency $\bar{\beta}$ as function of surface location on two-dimensional body for faired-type droplet distribution.

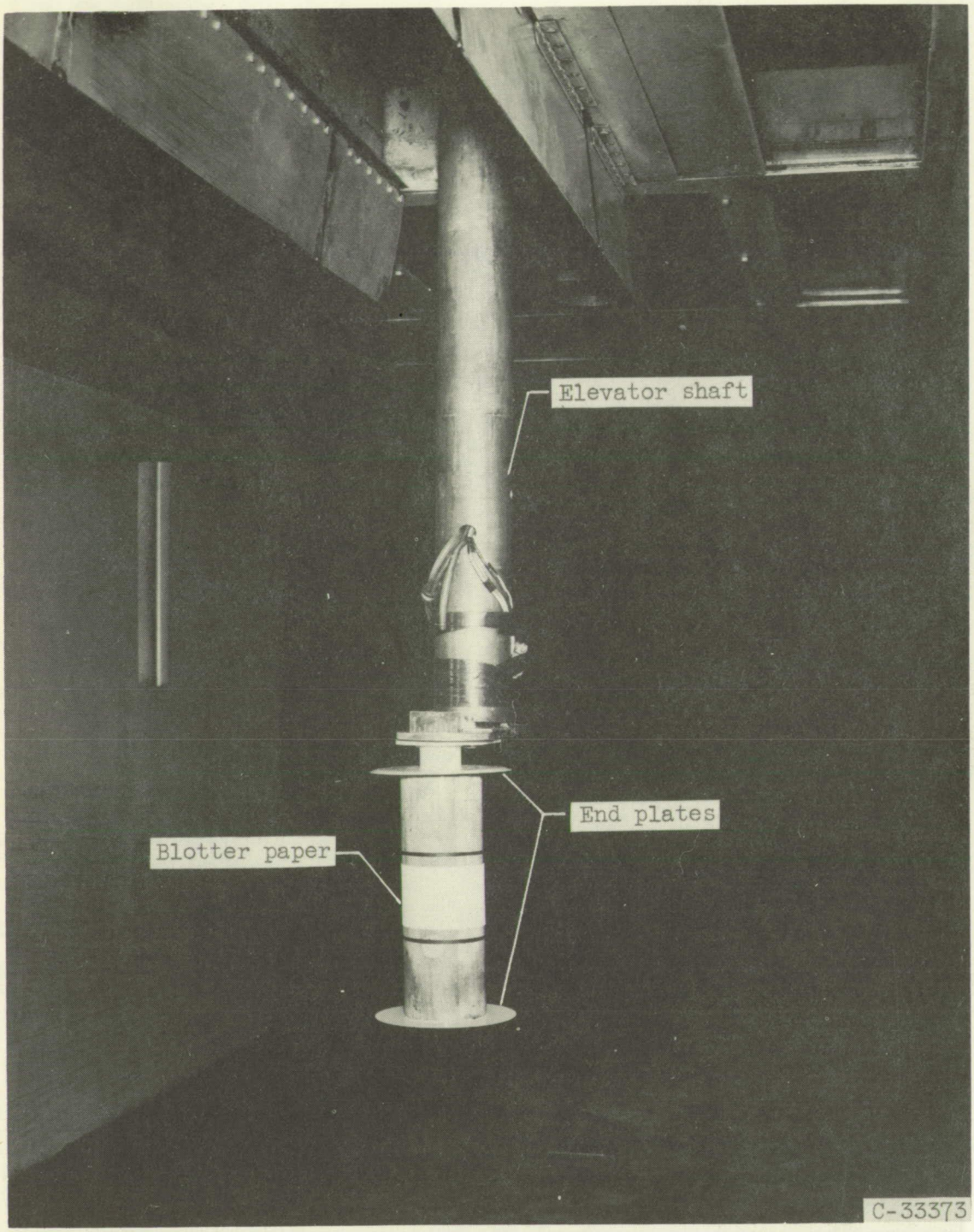

Figure 9. - Typical installation of cylinder (4-in. diam.), with blotter attached, in 6- by 9-foot test section of icing tunnel (looking downstream).

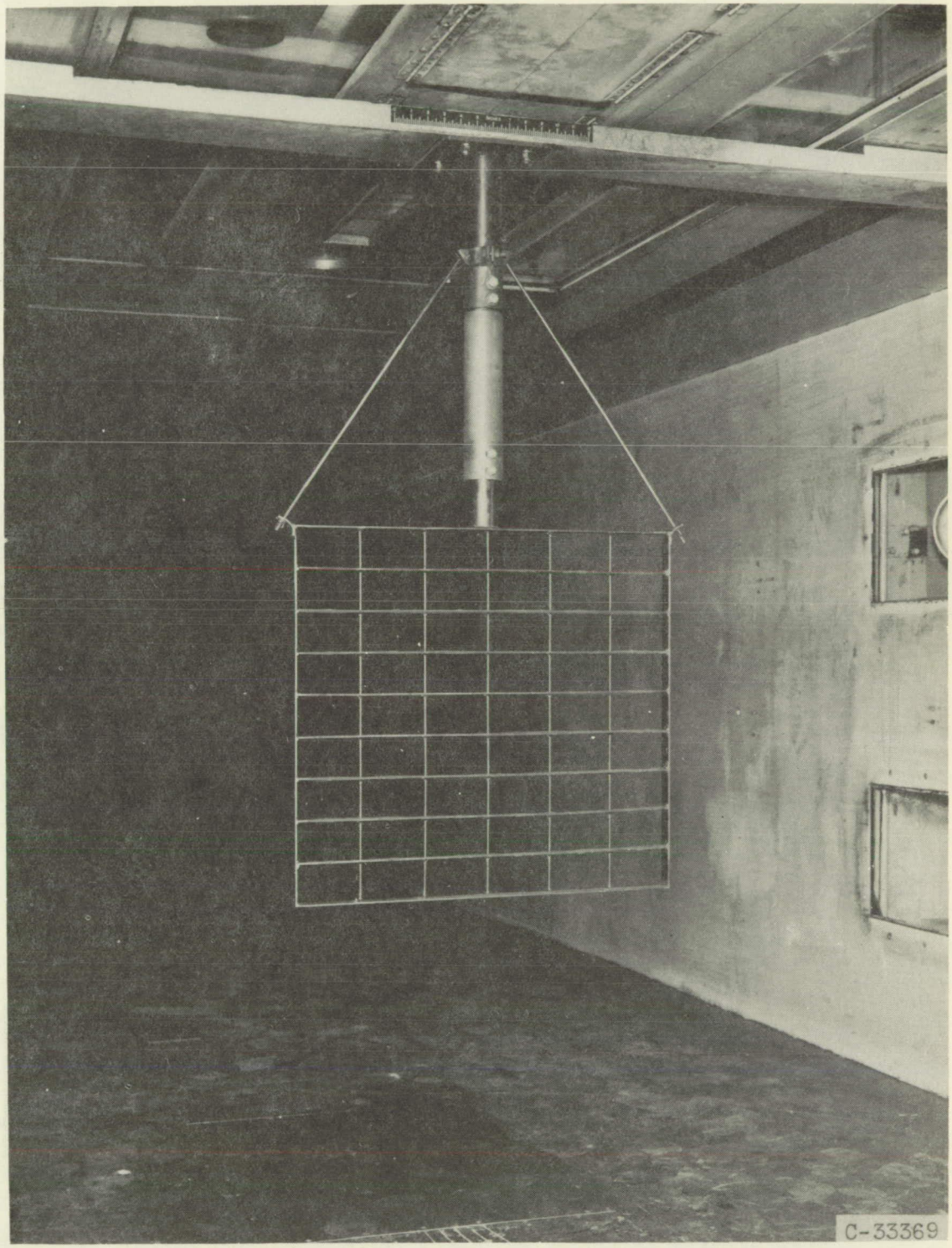

Figure 10. - Installation of grid used for mounting ribbons to measure uniformity of spray cloud in 6- by 9-foot test section of icing tunnel (looking downstream).

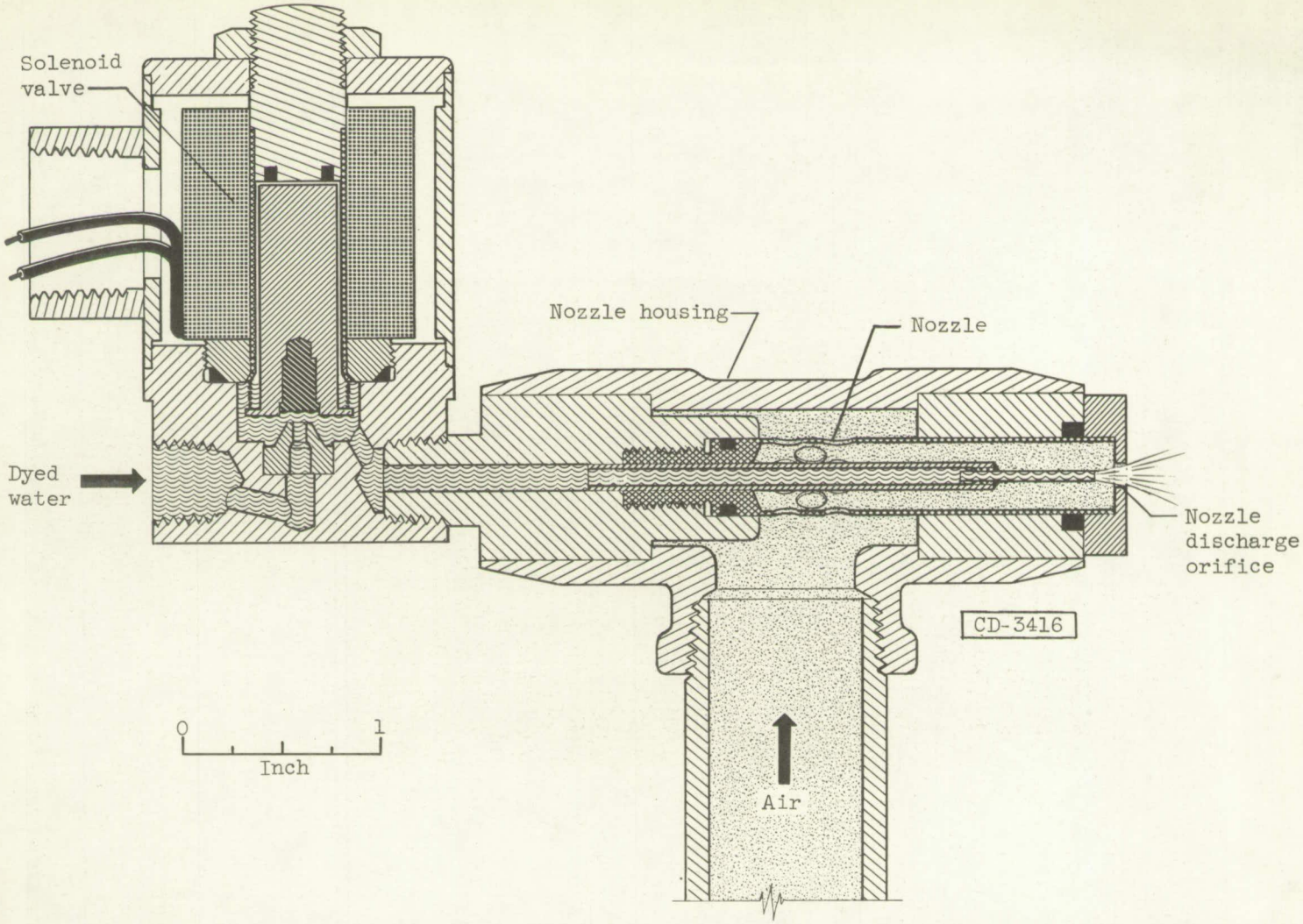

Figure 11. - Cross section of air-water atomizing-nozzle assembly.

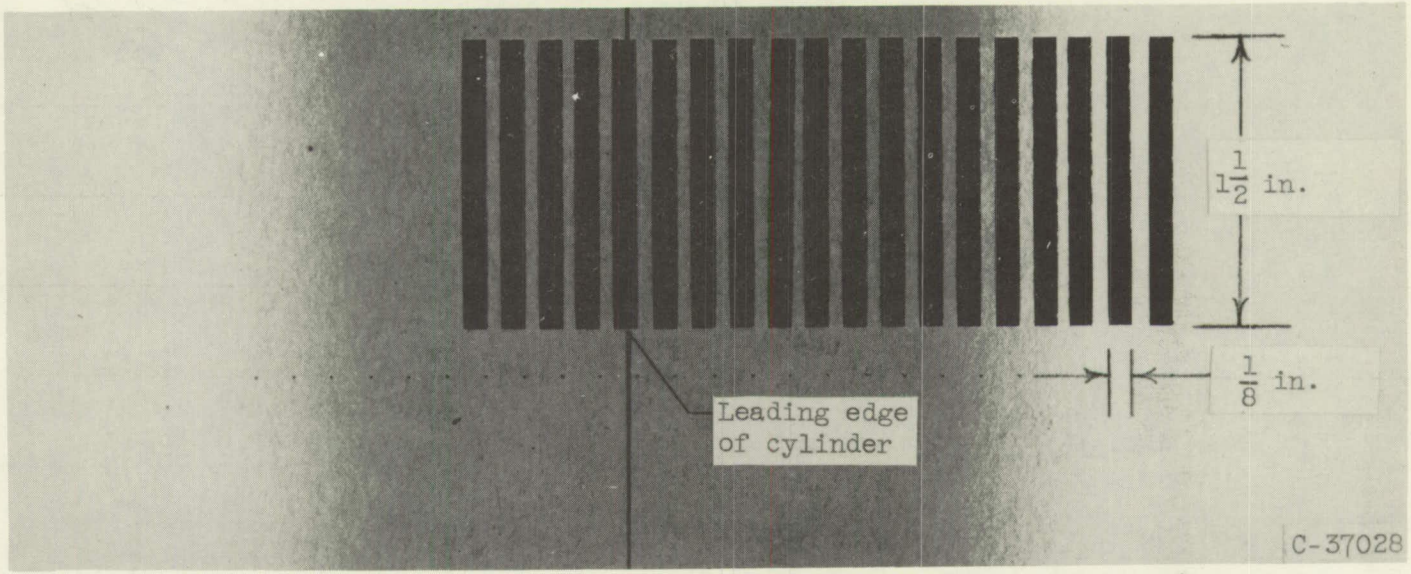

Figure 12. - Typical blotter record from cylinder with punched segments removed for colorimetric analysis after exposure to dyed-water cloud.

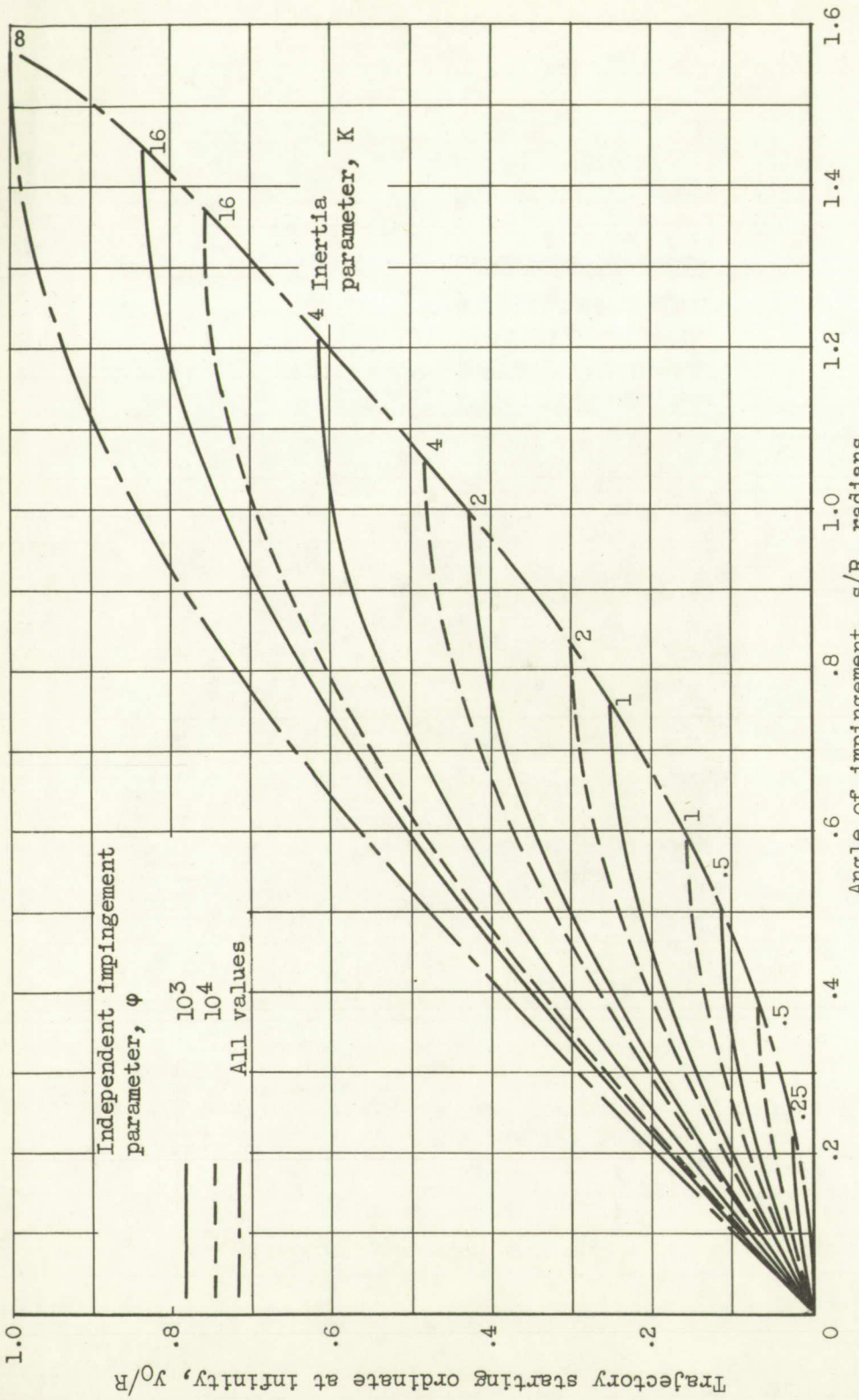

Figure 13. - Trajectory starting ordinates as function of angle of impingement for cylinder (ref. 1).

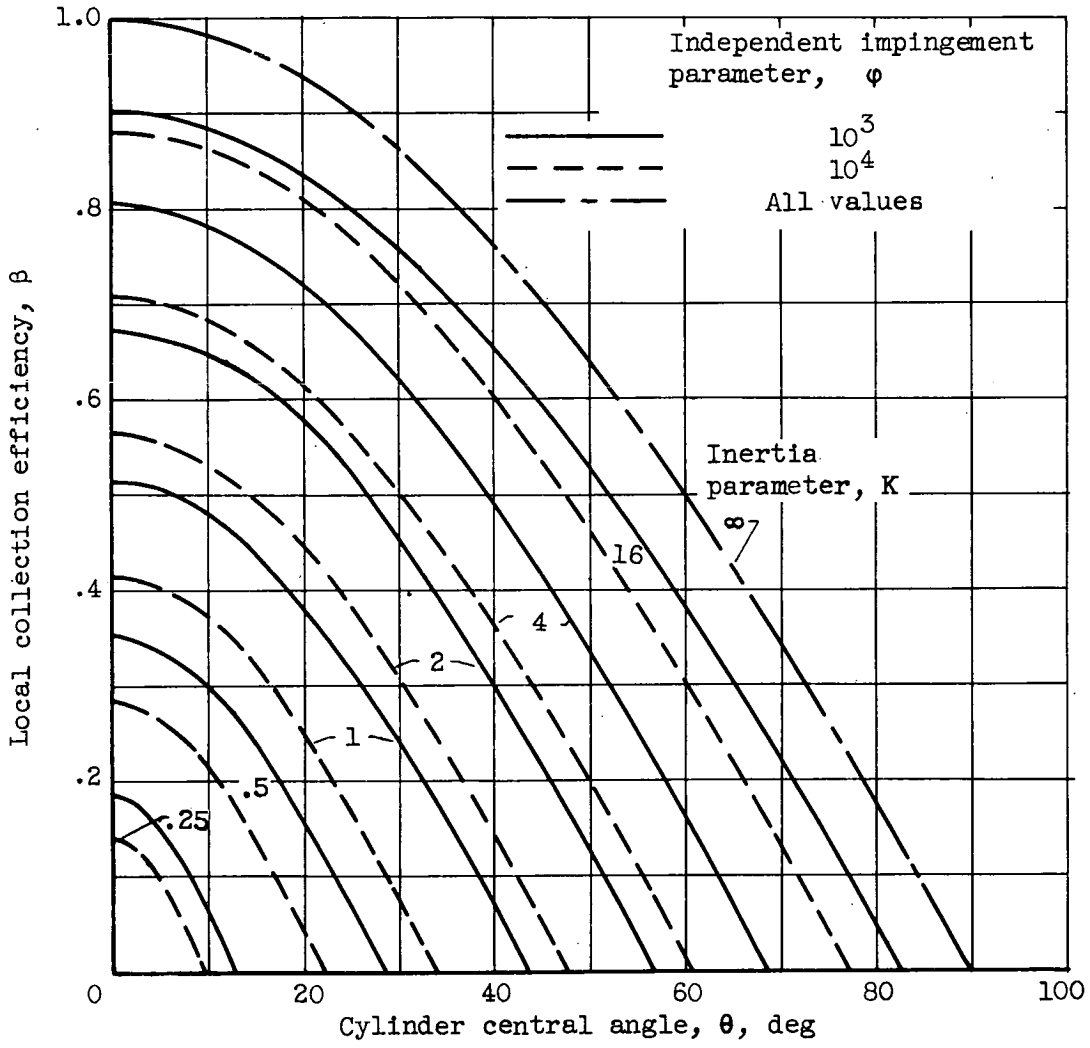

Figure 14. - Local collection efficiency for cylinder as function of central angle (ref. 1).

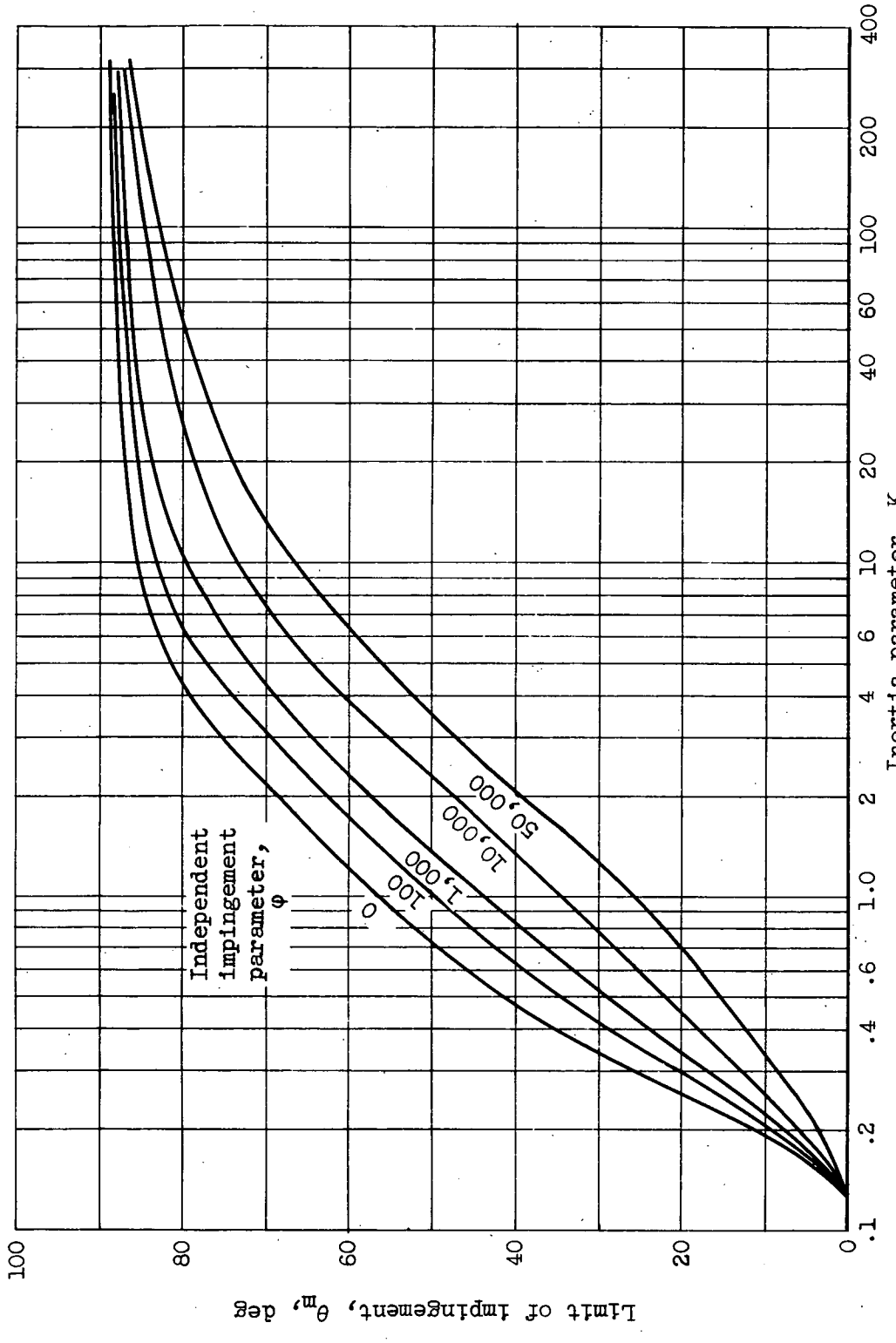

Figure 15. - Limit of impingement on cylinder (ref. 1).

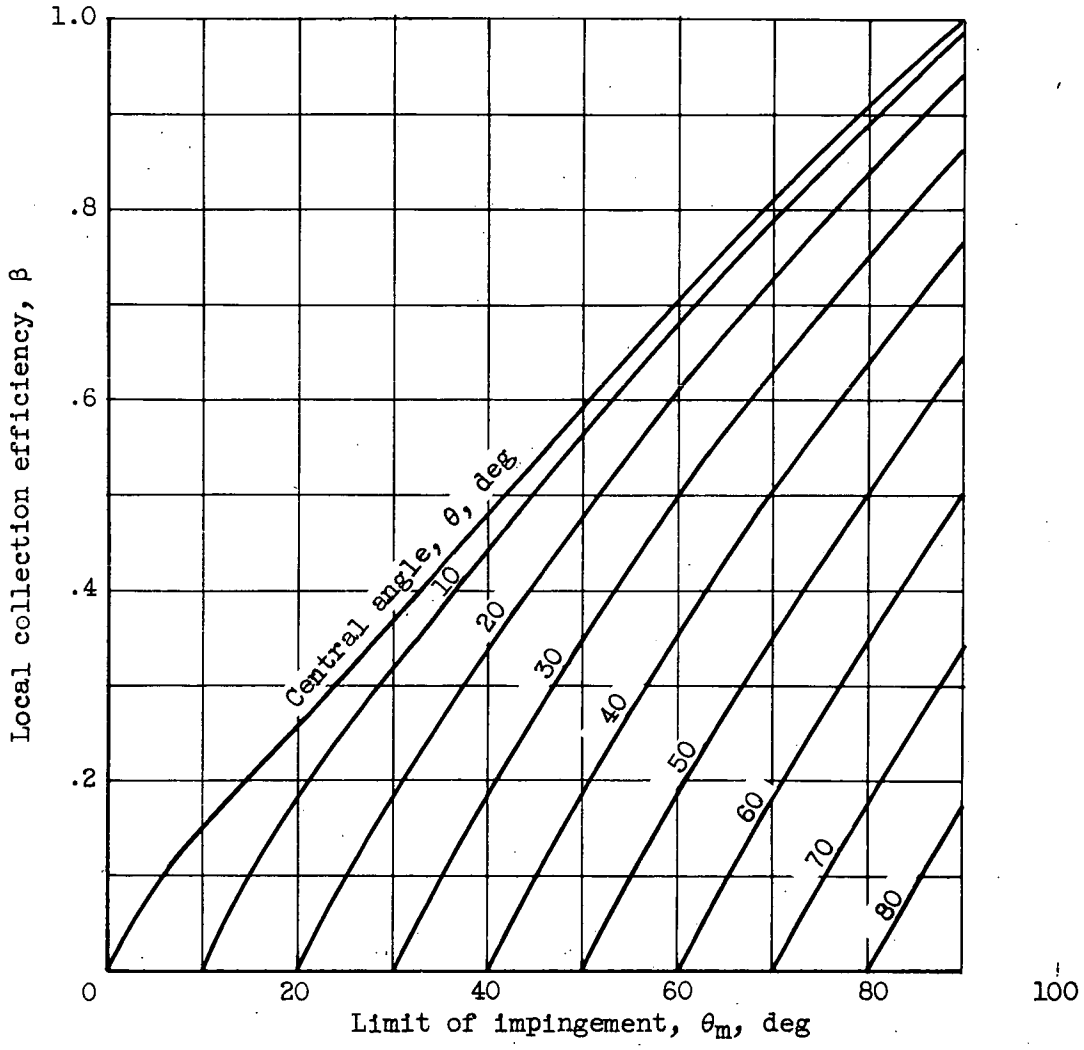

Figure 16. - Local collection efficiency (average for independent impingement parameter $\varphi = 10^3$ and 10^4) as function of central angle θ and limit of impingement θ_m (ref. 1).

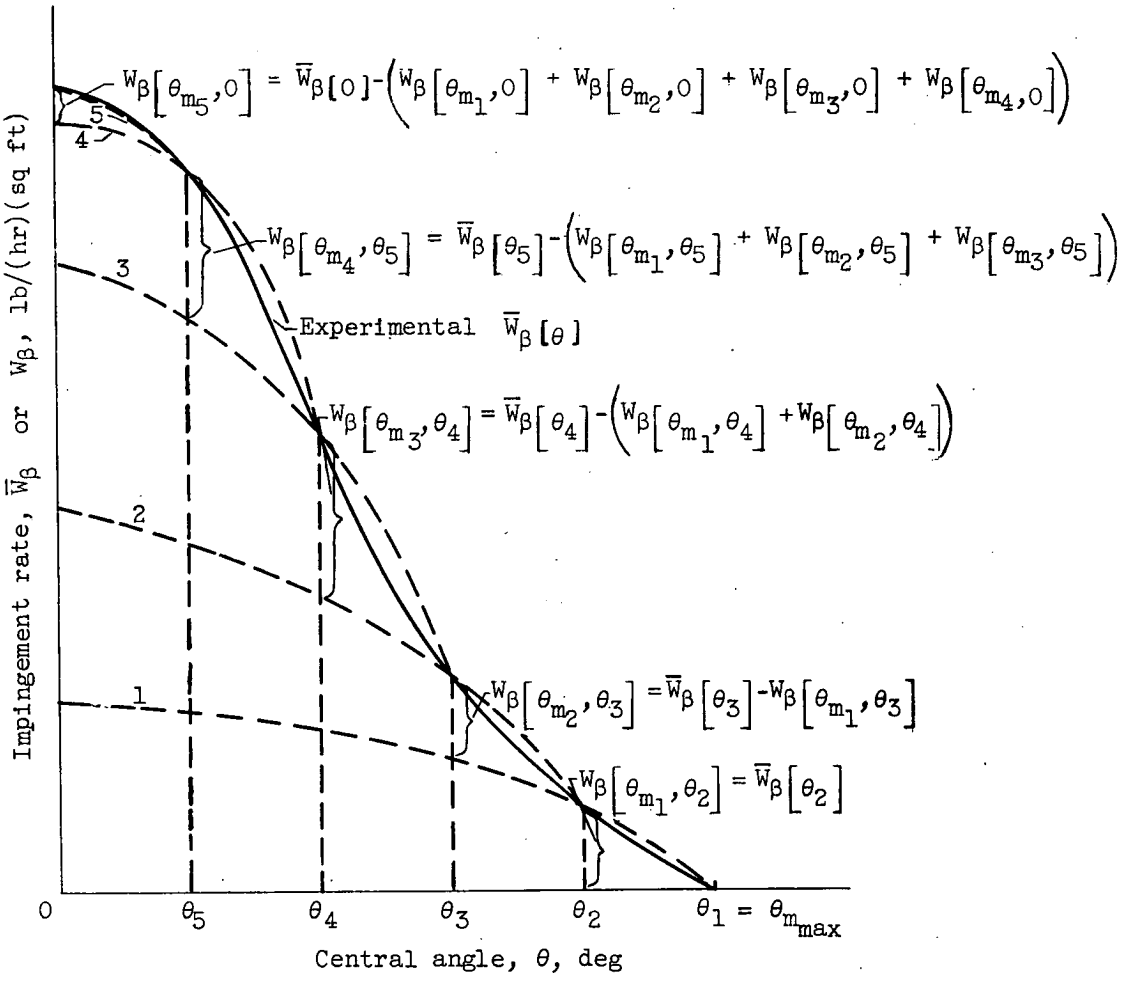

Figure 17. - Typical experimental impingement rate for cylinder showing arbitrary increments of central angle θ and including contributions of several droplet size groups.

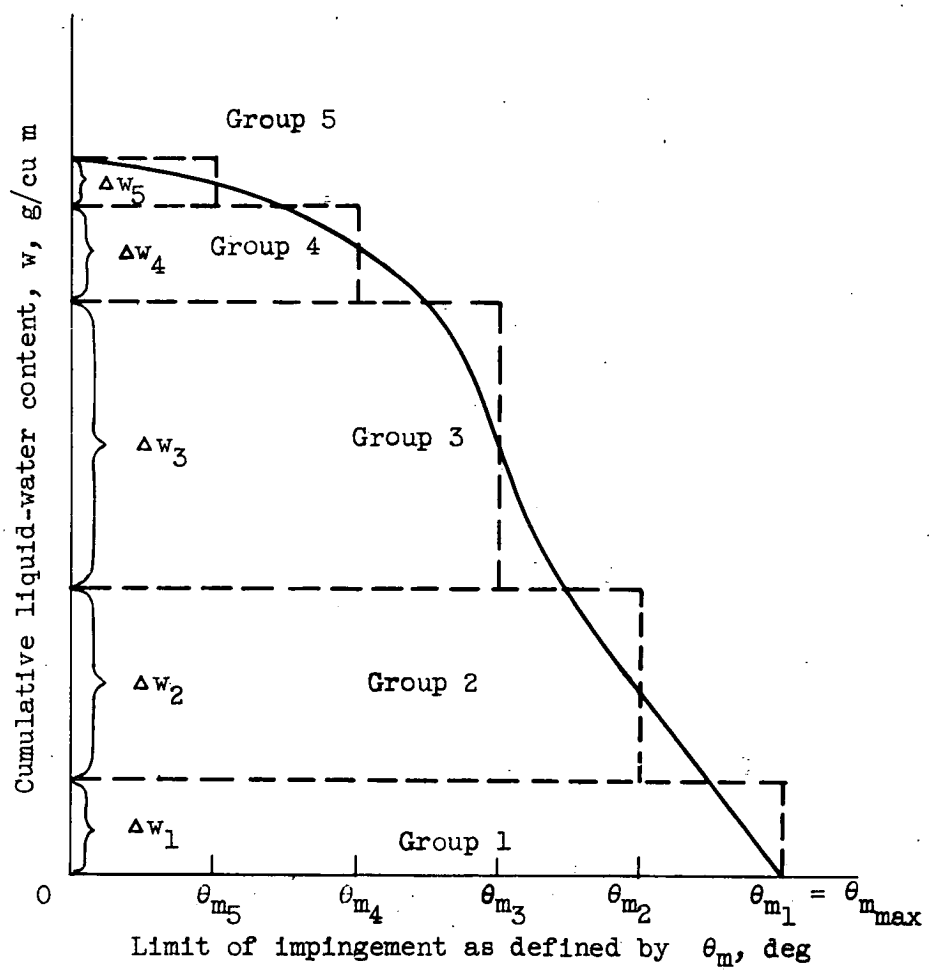

Figure 18. - Block- and faired-type droplet size distributions as specified by limit of impingement θ_m on cylinder and cumulative liquid-water content w.

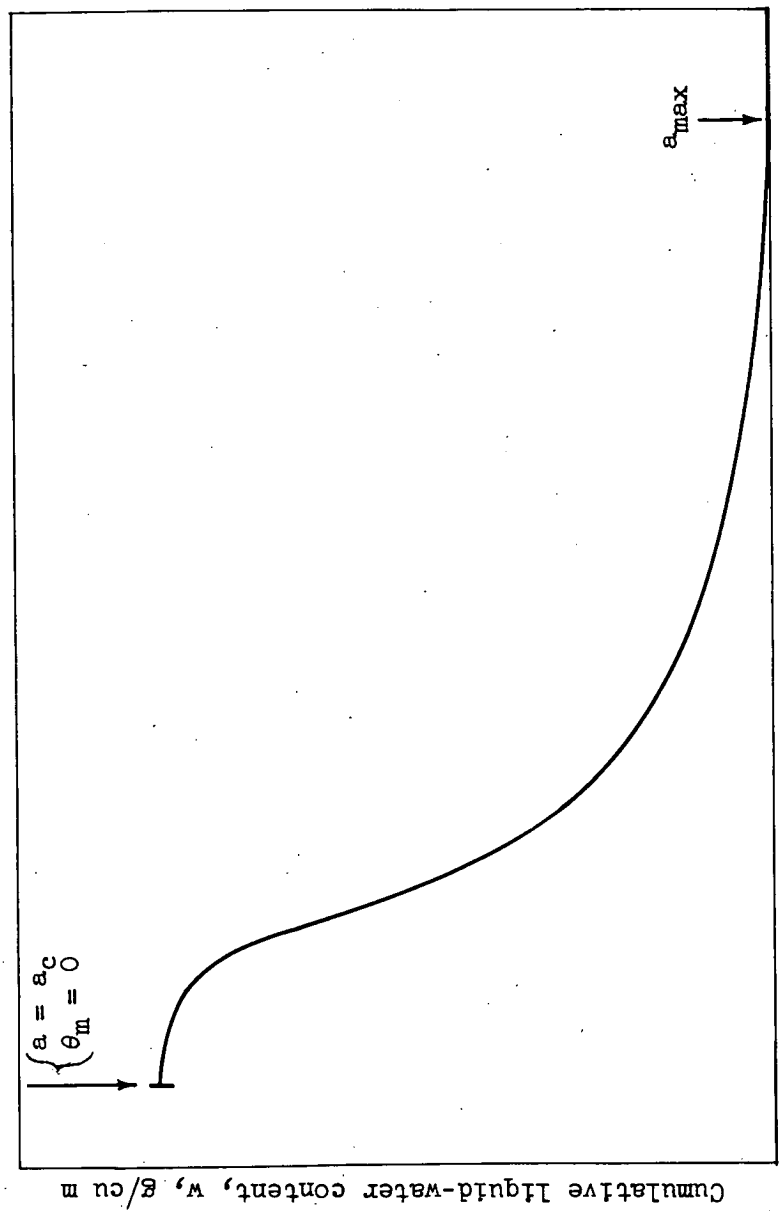

Figure 19. - Typical variation of liquid-water content with droplet radius from analytical solution of impingement rates on cylinders.

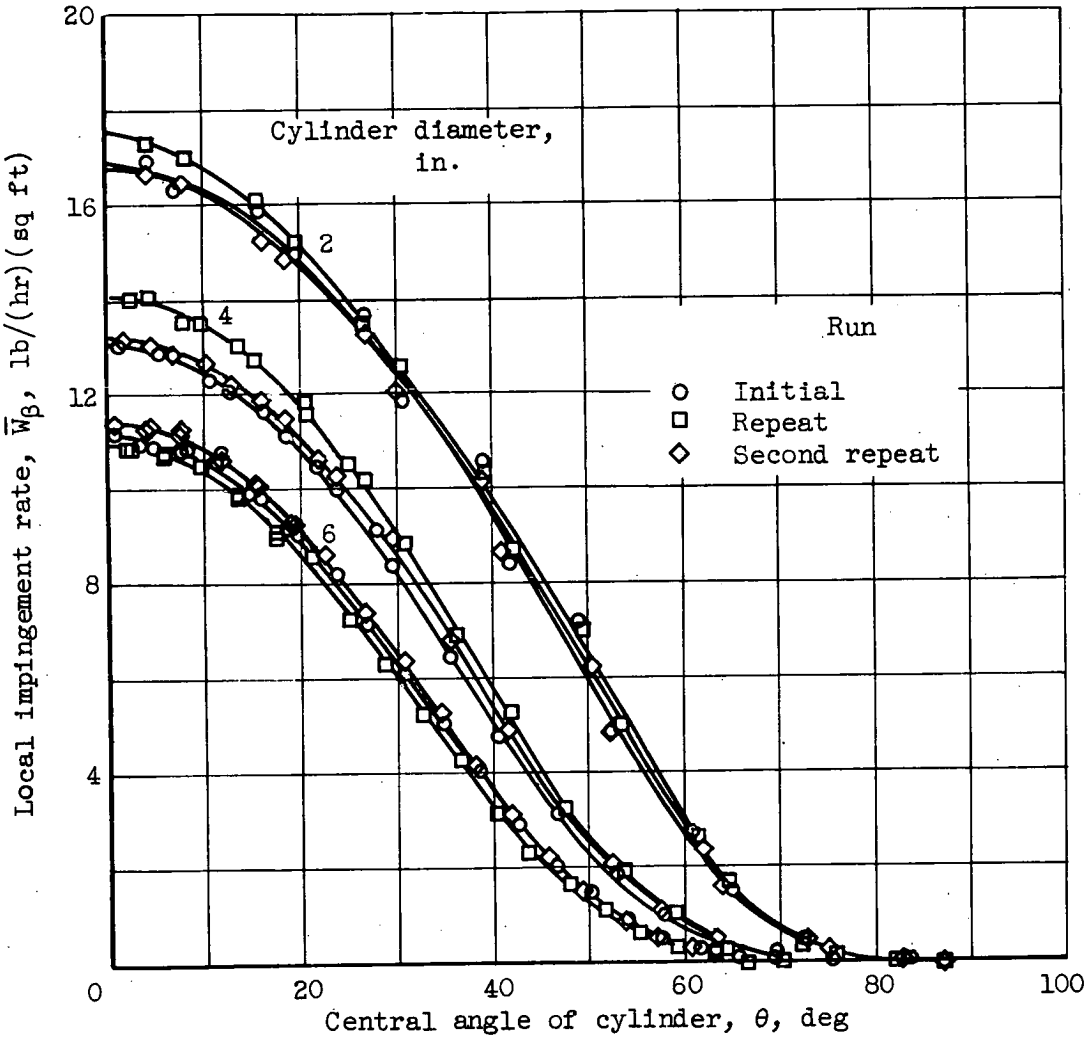

(a) Air-water pressure ratio, 0.5 (60 psi air to 120 psi water).

Figure 20. - Experimental local water impingement rates for three cylinder sizes. Airspeed, 175 miles per hour.

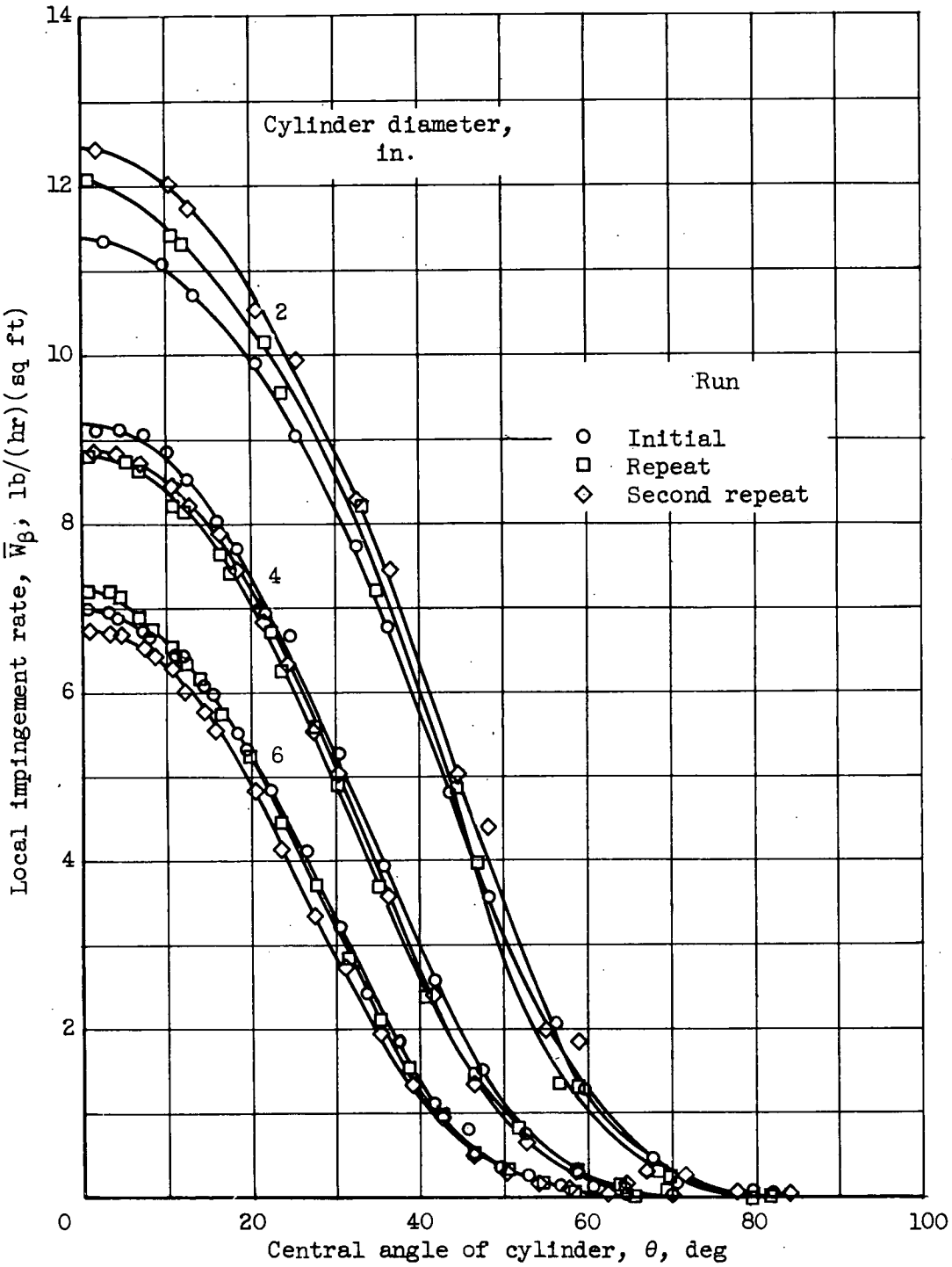

(b) Air-water pressure ratio, 0.6 (60 psi air to 100 psi water).

Figure 20. - Continued. Experimental local water impingement rates for three cylinder sizes. Airspeed, 175 miles per hour.

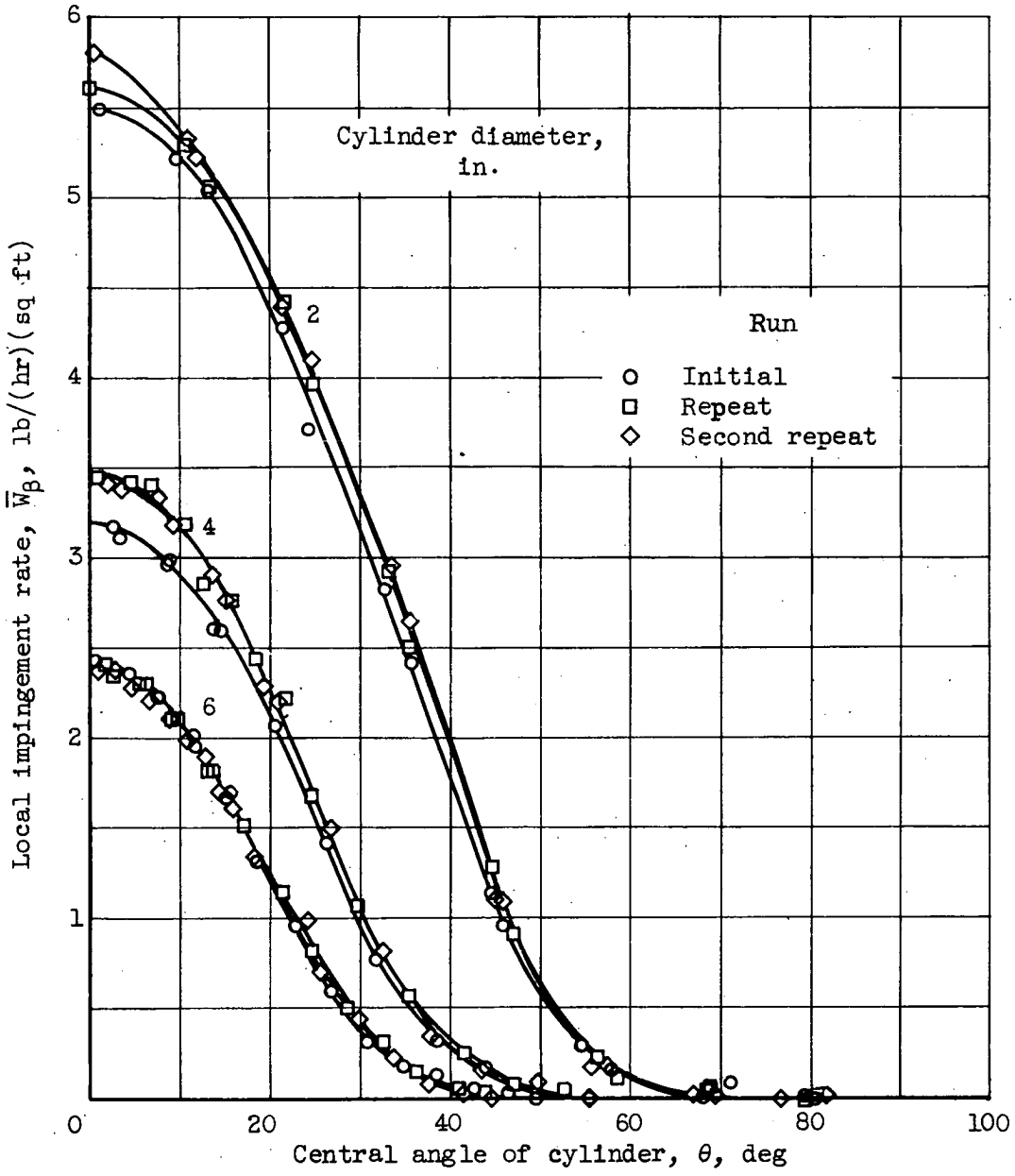

(c) Air-water pressure ratio, 0.8 (80 psi air to 100 psi water).

Figure 20. - Concluded. Experimental local water impingement rates for three cylinder sizes. Airspeed, 175 miles per hour.

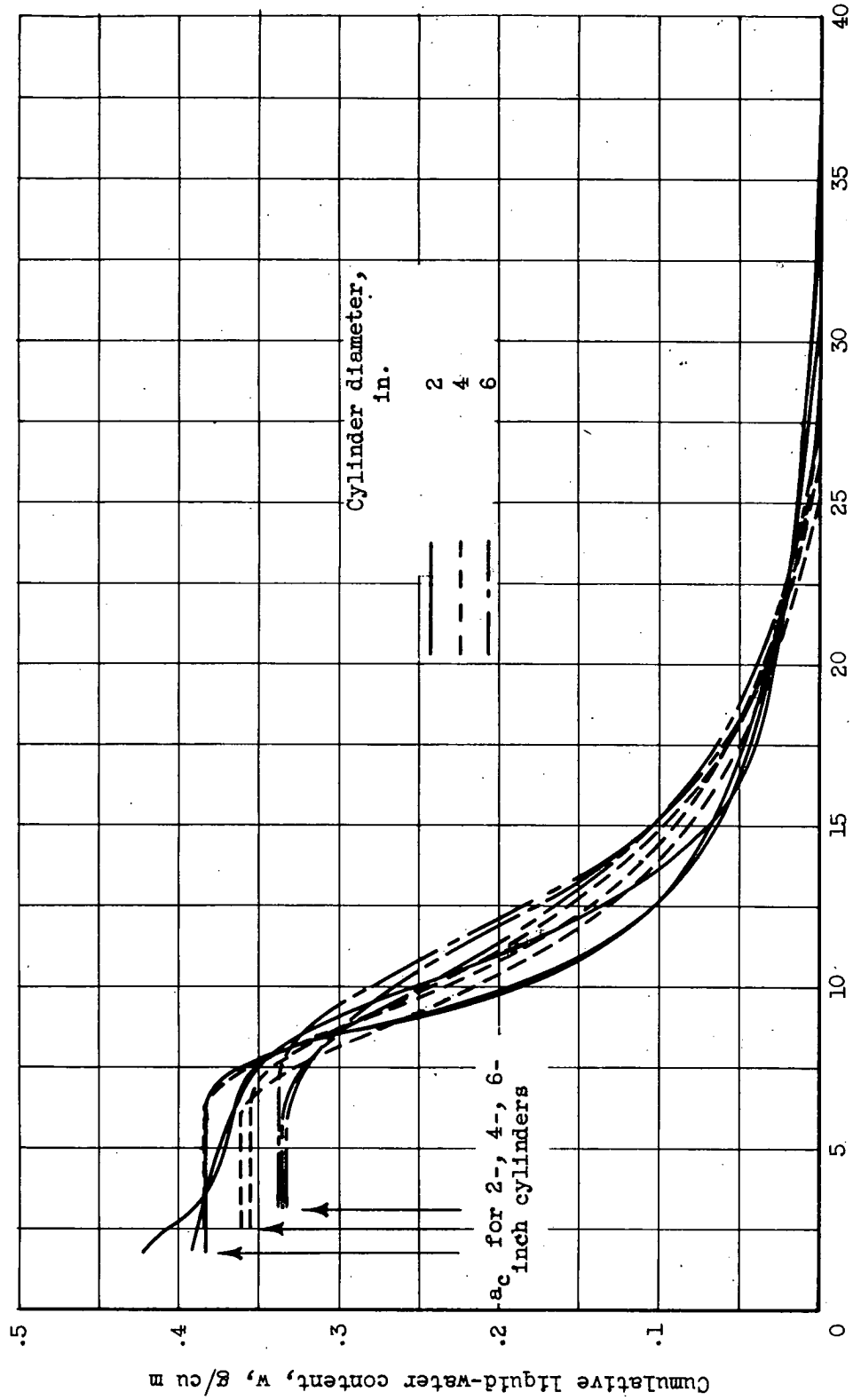

(a) Air-water pressure ratio, 0.5 (60 psi air to 120 psi water).

Figure 21. - Droplet size distribution obtained from experimental impingement rates on cylinders (based on theoretical trajectories from ref. 1).

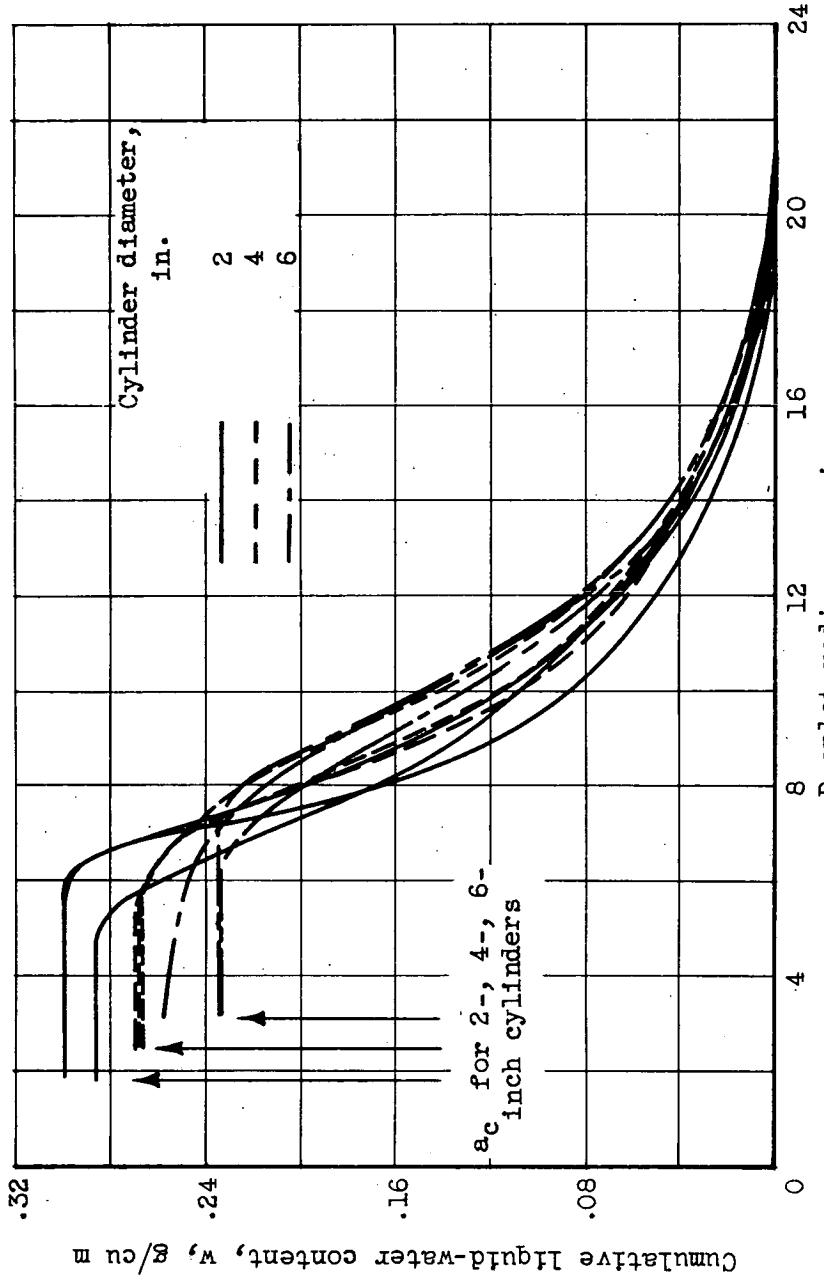

(b) Air-water pressure ratio, 0.6 (60 psi air to 100 psi water).

Figure 21. - Continued. Droplet size distribution obtained from experimental impingement rates on cylinders (based on theoretical trajectories from ref. 1).

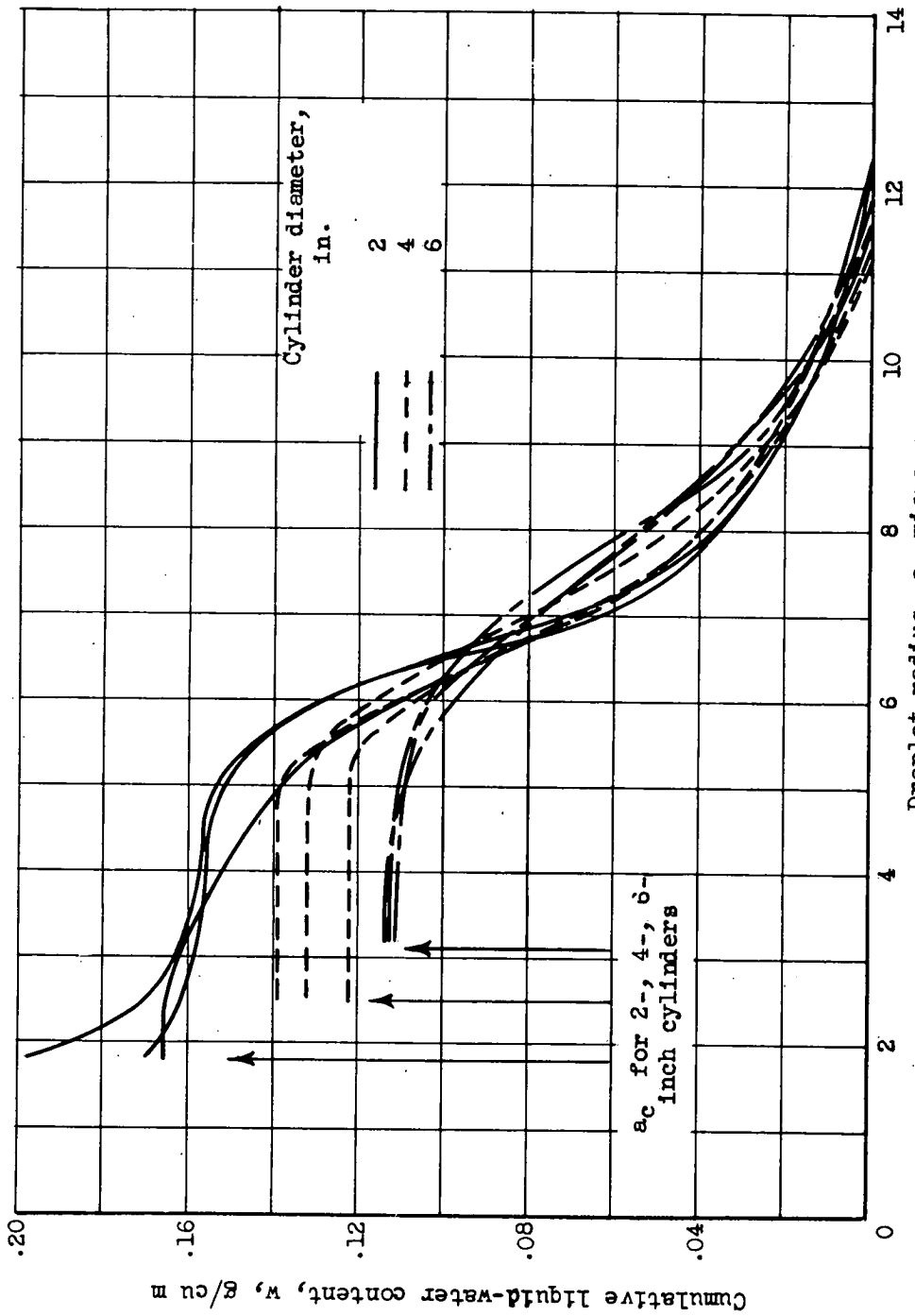

(c) Air-water pressure ratio, 0.8 (80 psi air and 100 psi water).

Figure 21. - Concluded. Droplet size distribution obtained from experimental impingement rates on cylinders (based on theoretical trajectories from ref. 1).

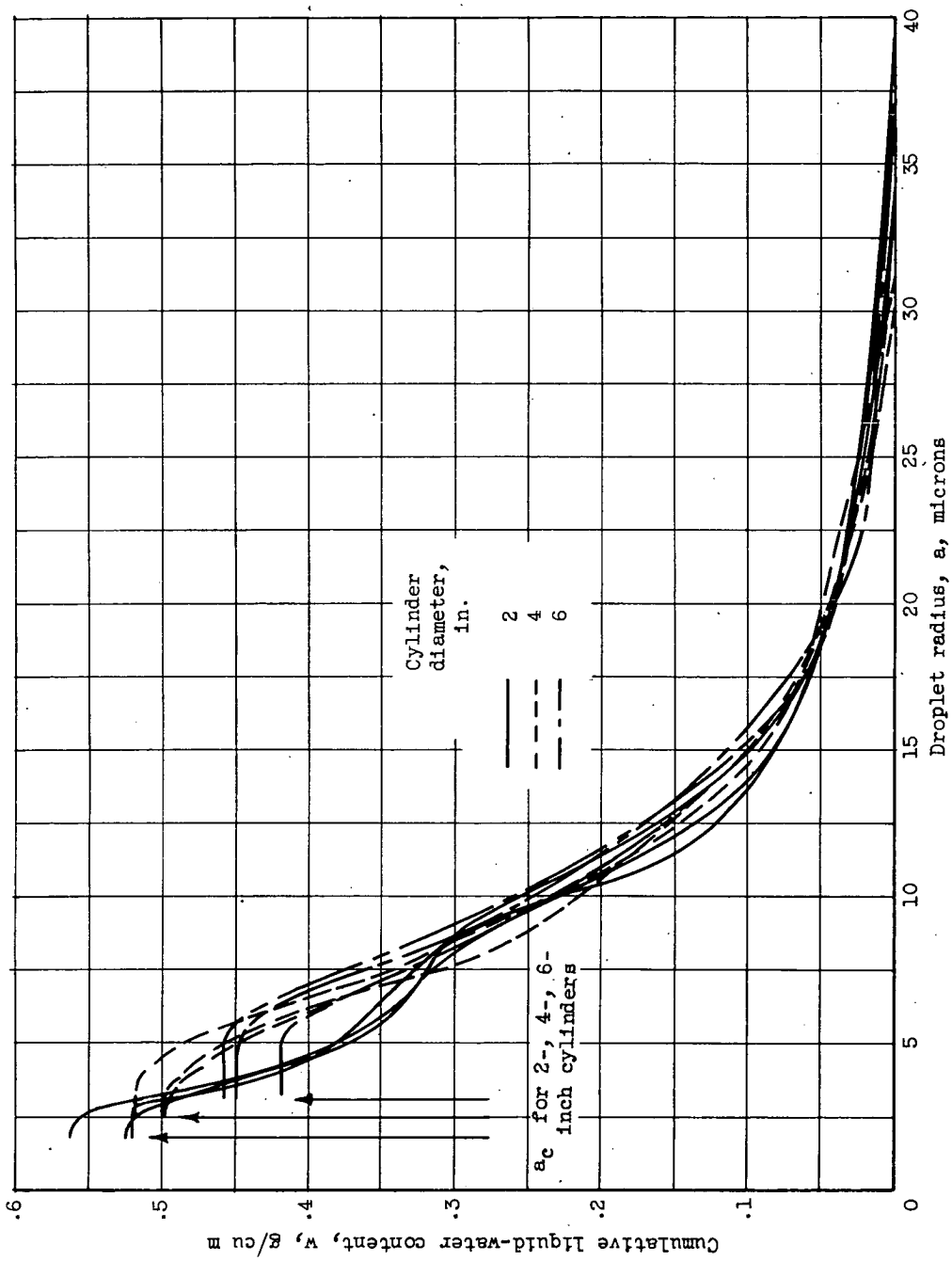

(a) Air-water pressure ratio, 0.5 (60 psi air to 120 psi water).

Figure 22. - Droplet size distribution obtained from experimental impingement rates on cylinders (based on theoretical trajectories from ref. 2).

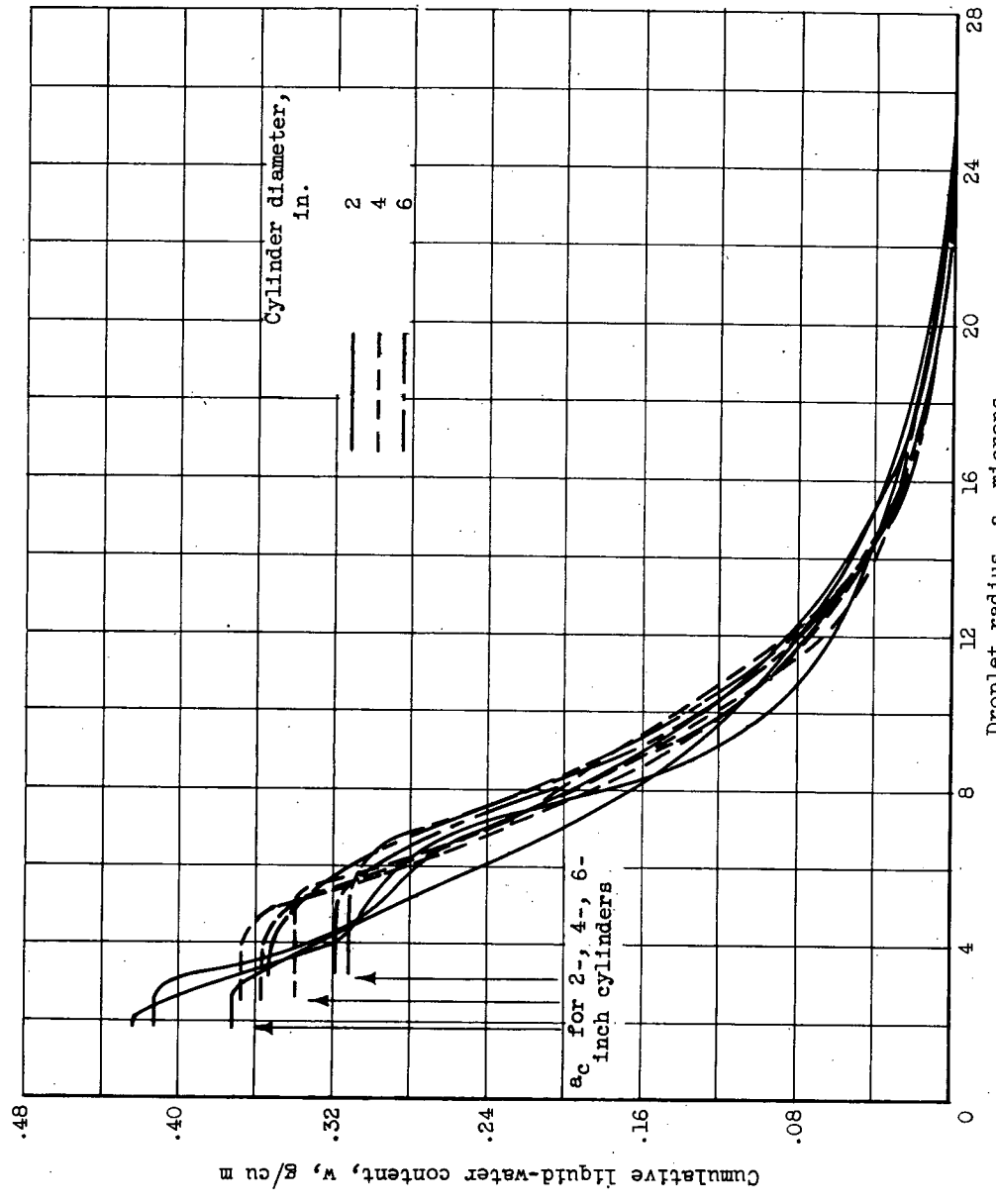

(b) Air-water pressure ratio, 0.6 (60 psi air to 100 psi water).

Figure 22. - Continued. Droplet size distribution obtained experimental impingement rates on cylinders (based on theoretical trajectories from ref. 2).

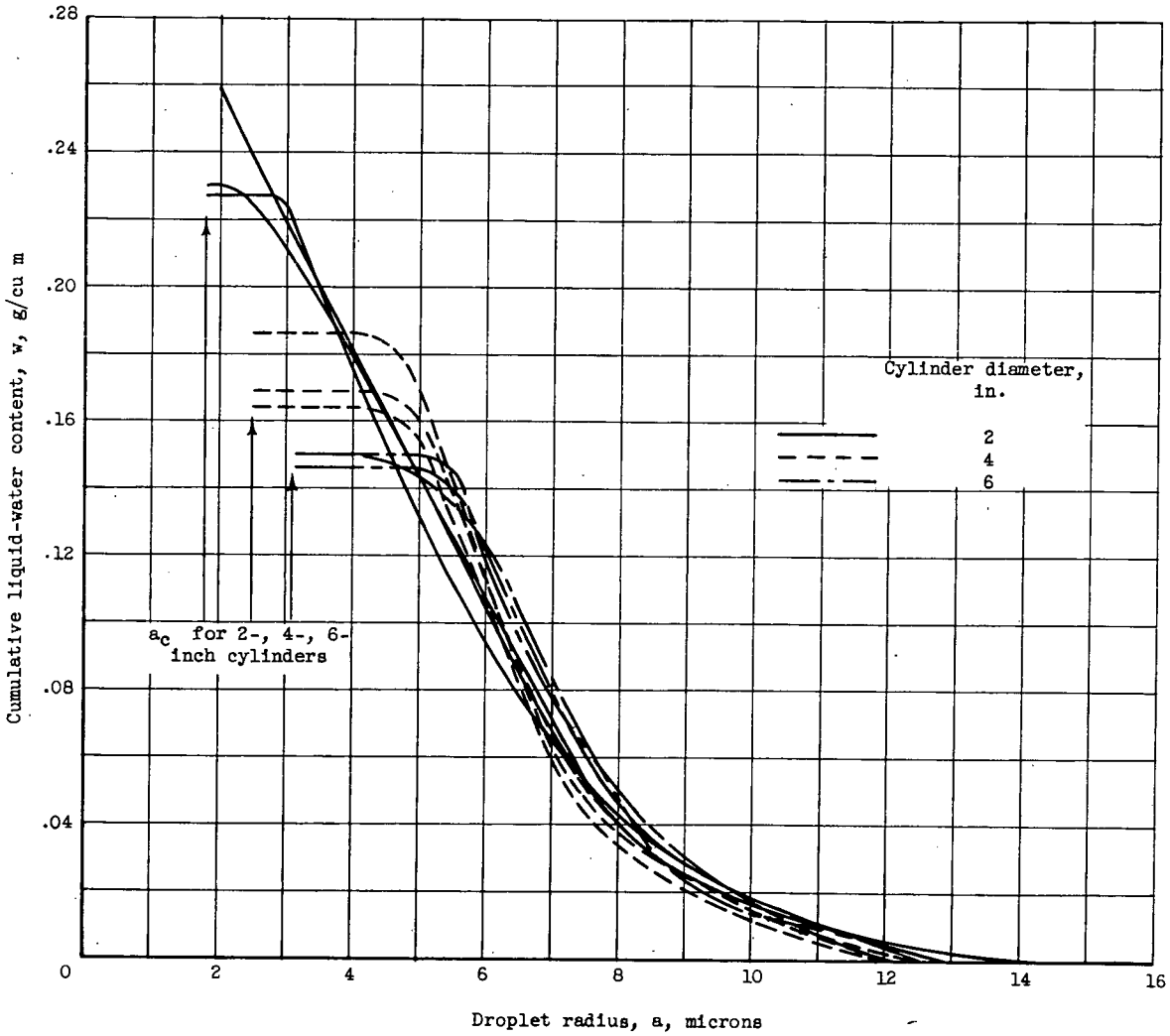

(c) Air-water pressure ratio, 0.8 (80 psi air to 100 psi water).

Figure 22. - Concluded. Droplet size distribution obtained from experimental impingement rates on cylinders (based on theoretical trajectories from ref. 2).

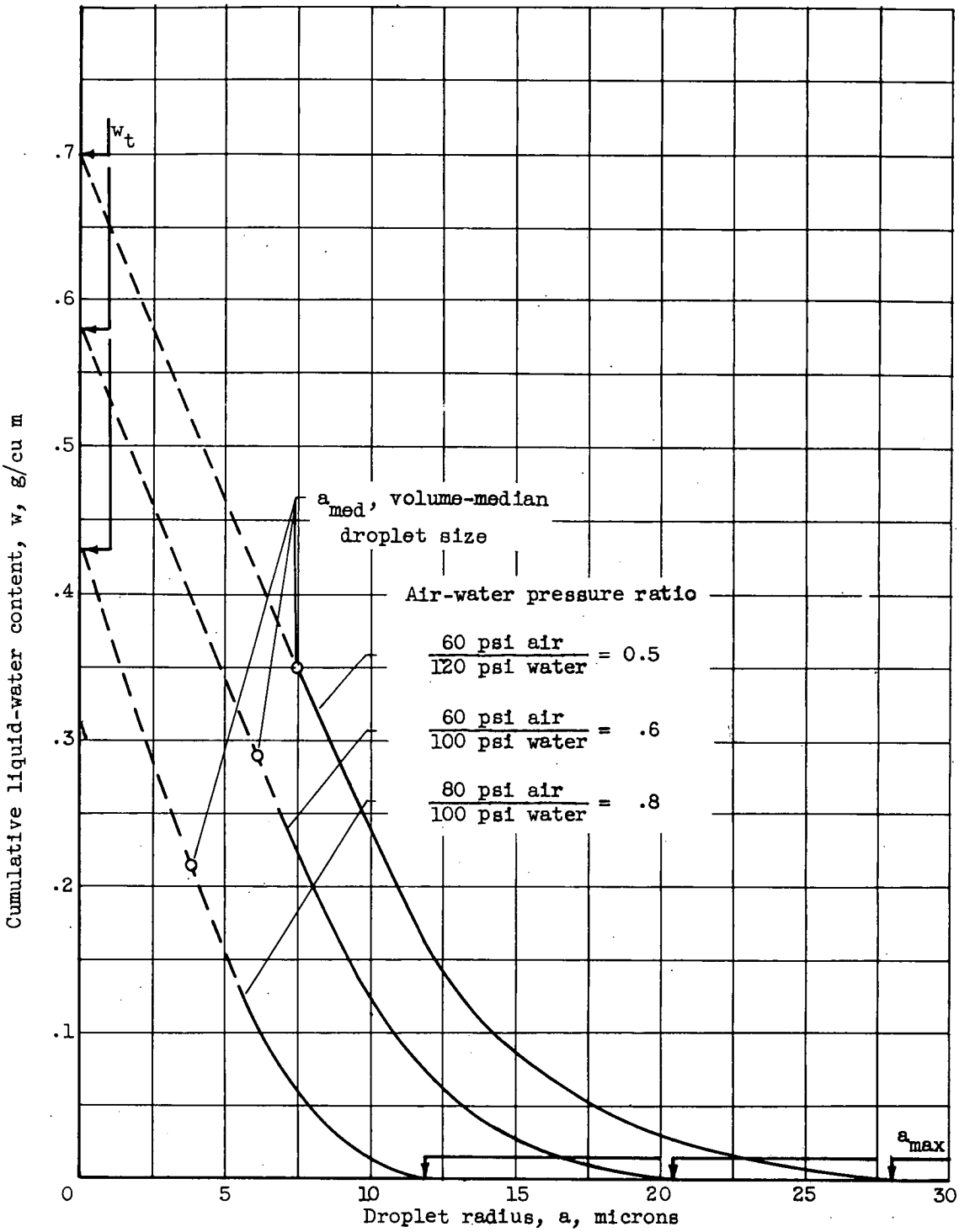

Figure 23. - Final evaluation of droplet size distribution for three spray conditions based on experimental impingement rates of cylinders and an aspirating device (based on theoretical trajectories from ref. 1).

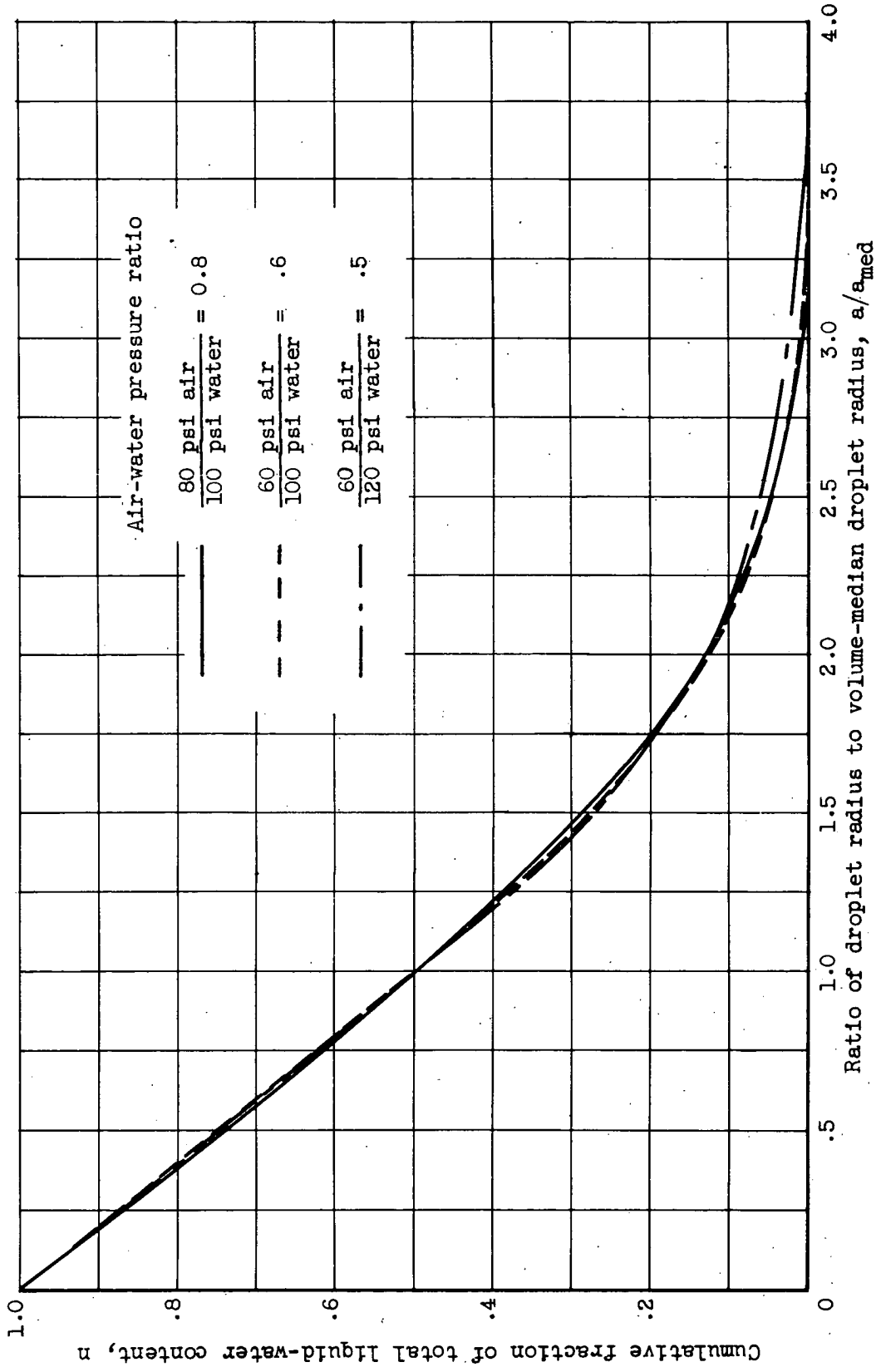

Figure 24. - Dimensionless droplet size distribution obtained experimentally for three spray conditions (based on theoretical trajectories from ref. 1).

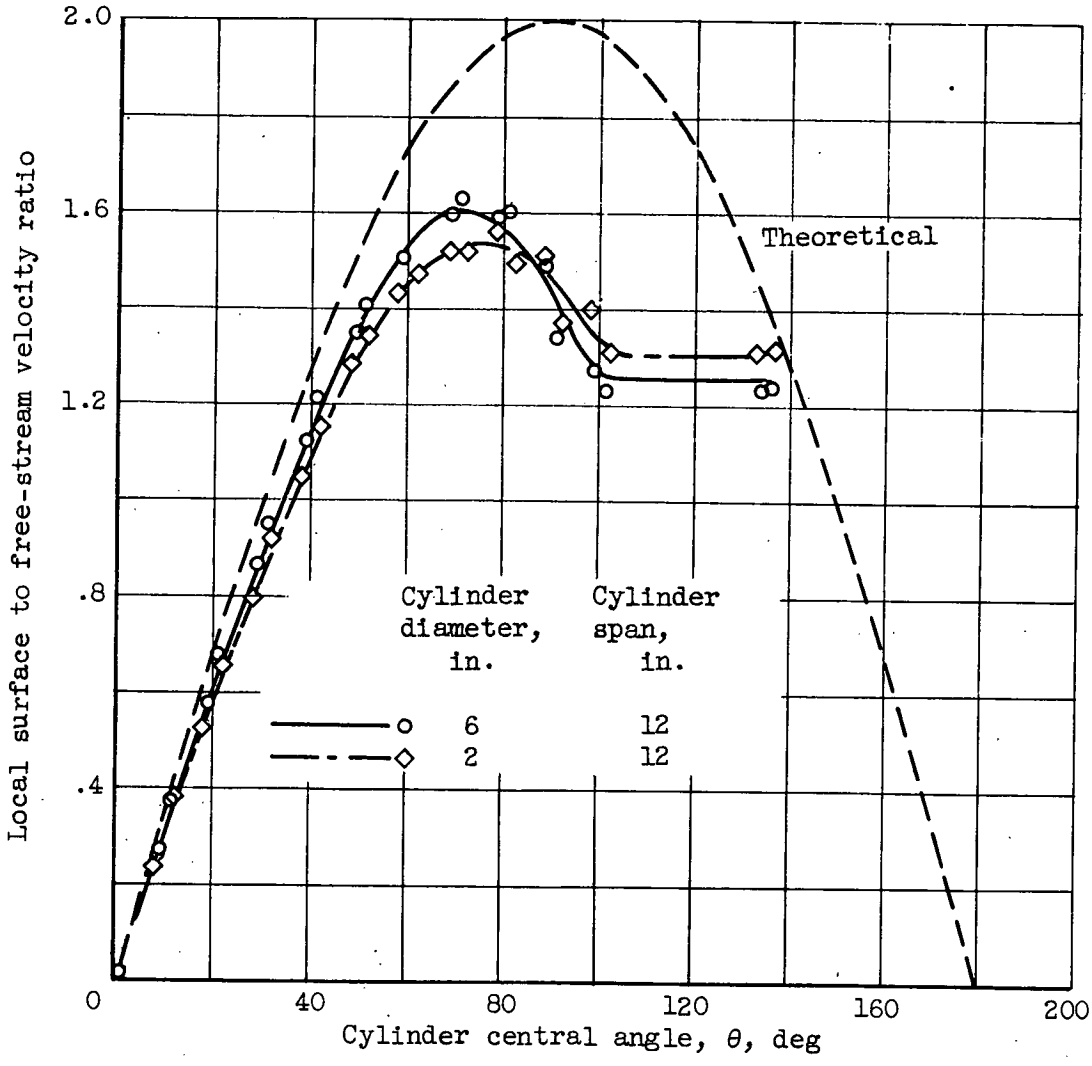

Figure 25. - Comparison of experimental (icing tunnel) with theoretical surface to free-stream velocity ratio for 6-inch- and 2-inch-diameter cylinders. Free-stream velocity, 175 miles per hour.

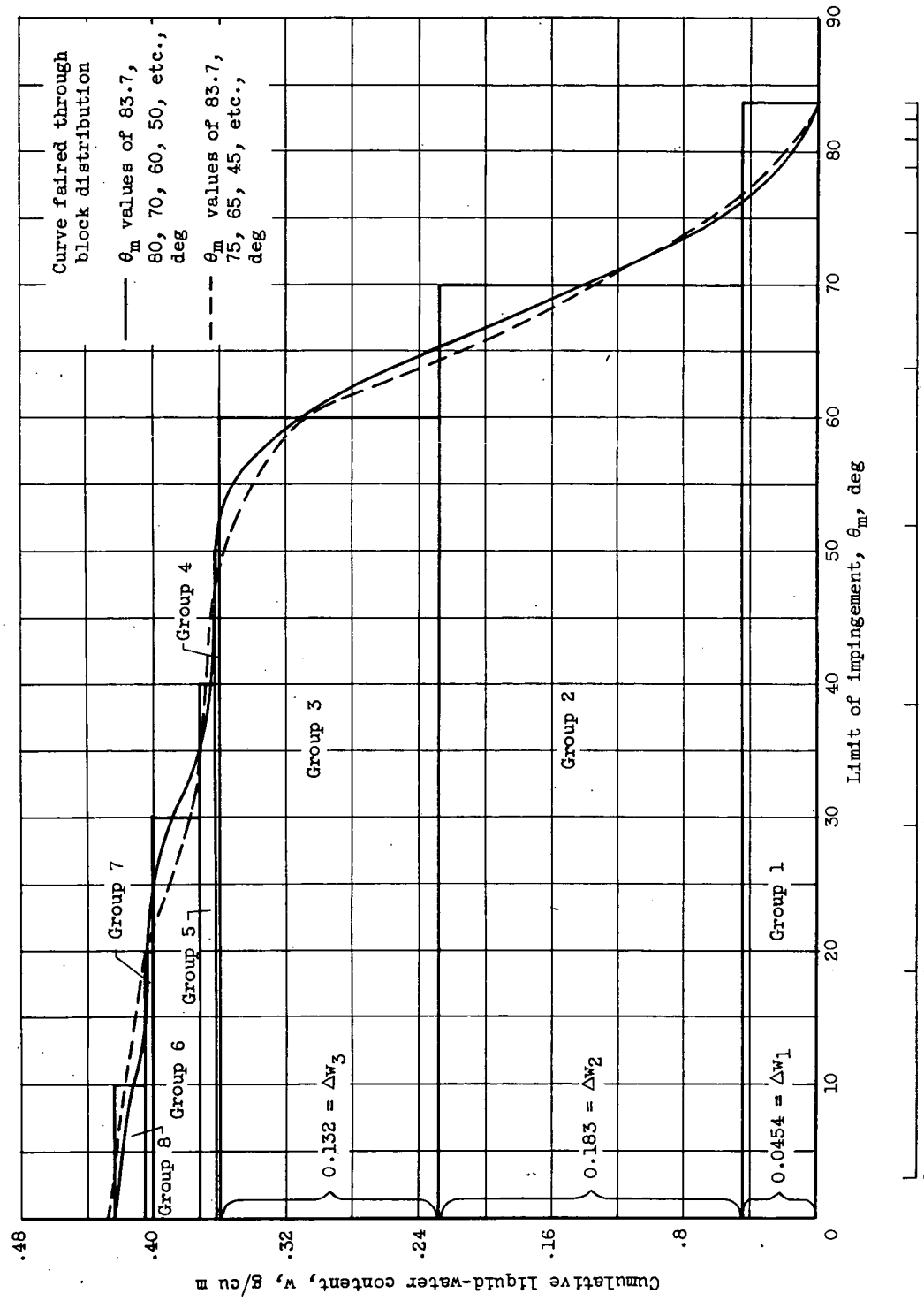

Figure 26. - Block- and faired-type droplet size distribution as specified by limit of impingement θ_m (also droplet radius a) and cumulative liquid-water content w from numerical example in appendix C.